



**ANALYSIS AND NUMERICAL SOLUTION
OF AN INTEGRAL EQUATION METHOD
FOR ELECTROMAGNETIC SCATTERING
FROM A CAVITY IN A GROUND PLANE**

THESIS

Eric T. Howe

AFIT/GAM/ENC/01S-1

DEPARTMENT OF THE AIR FORCE
AIR UNIVERSITY

AIR FORCE INSTITUTE OF TECHNOLOGY

Wright-Patterson Air Force Base, Ohio

APPROVED FOR PUBLIC RELEASE; DISTRIBUTION UNLIMITED.

20011221 000

REPORT DOCUMENTATION PAGE				Form Approved OMB No. 0704-0188	
The public reporting burden for this collection of information is estimated to average 1 hour per response, including the time for reviewing instructions, searching existing data sources, gathering and maintaining the data needed, and completing and reviewing the collection of information. Send comments regarding this burden estimate or any other aspect of this collection of information, including suggestions for reducing the burden, to Department of Defense, Washington Headquarters Services, Directorate for Information Operations and Reports (0704-0188), 1215 Jefferson Davis Highway, Suite 1204, Arlington, VA 22202-4302. Respondents should be aware that notwithstanding any other provision of law, no person shall be subject to any penalty for failing to comply with a collection of information if it does not display a currently valid OMB control number.					
PLEASE DO NOT RETURN YOUR FORM TO THE ABOVE ADDRESS.					
1. REPORT DATE (DD-MM-YYYY) 04-09-2001		2. REPORT TYPE Master's Thesis		3. DATES COVERED (From - To) September 1999 - August 2001	
4. TITLE AND SUBTITLE Analysis and Numerical Solution of an Integral Equation Method for Electromagnetic Scattering From a Cavity in a Ground Plane				5a. CONTRACT NUMBER	
				5b. GRANT NUMBER	
				5c. PROGRAM ELEMENT NUMBER	
				5d. PROJECT NUMBER	
6. AUTHOR(S) Eric T. Howe				5e. TASK NUMBER	
				5f. WORK UNIT NUMBER	
7. PERFORMING ORGANIZATION NAME(S) AND ADDRESS(ES) Air Force Institute of Technology Graduate School of Engineering and Management (AFIT/EN) 2950 P Street, Building 640 WPAFB, OH 45433-7765				8. PERFORMING ORGANIZATION REPORT NUMBER AFIT/GAM/ENC/01S-1	
9. SPONSORING/MONITORING AGENCY NAME(S) AND ADDRESS(ES) Air Force Institute of Technology Graduate School of Engineering and Management (AFIT/EN) 2950 P Street, Building 640 WPAFB, OH 45433-7765				10. SPONSOR/MONITOR'S ACRONYM(S)	
				11. SPONSOR/MONITOR'S REPORT NUMBER(S)	
12. DISTRIBUTION/AVAILABILITY STATEMENT Approved for public release; distribution unlimited.					
13. SUPPLEMENTARY NOTES					
14. ABSTRACT <p>In this research the electromagnetic scattering of a plane wave from a two-dimensional cavity embedded in an infinite, perfectly conducting ground plane is investigated. The plane wave is assumed to be under transverse electric (TE) polarization with respect to the x-axis. The cavity may be empty or filled with an arbitrary homogeneous, lossy material. A coupled set of scalar integral equations that govern the electromagnetic scattering is implemented.</p> <p>An approximate solution to the scalar integral equations is found via a Method of Moments (MoM) algorithm. The algorithm is implemented in a computer code, and approximations to the total magnetic field on the cavity surface and aperture as well as the normal derivative of the total magnetic field on the cavity aperture are obtained. These fields are then used to calculate the two-dimensional monostatic RCS signatures of various test cavities.</p> <p>The numerical results from the algorithm are shown to agree well with the RCS signatures calculated by other well-known methods and published results. In addition to being accurate, the algorithm is very computationally efficient. The process results in simply solving a relatively small, well-conditioned matrix system for each incident angle to produce the unknown fields.</p>					
15. SUBJECT TERMS Electromagnetic Scattering, Two-Dimensional Cavity, TE Polarization, Method of Moments, Integral Equation Method					
16. SECURITY CLASSIFICATION OF:			17. LIMITATION OF ABSTRACT		18. NUMBER OF PAGES
a. REPORT Unclassified	b. ABSTRACT Unclassified	c. THIS PAGE Unclassified	UU		79
			19a. NAME OF RESPONSIBLE PERSON Dr. Aihua Wood, AFIT		
			19b. TELEPHONE NUMBER (Include area code) 937-255-3636 ext 4521		

The views expressed in this thesis are those of the author and do not reflect the official policy or position of the Department of Defense or the United States Government.

AFIT/GAM/ENC/01S-1

ANALYSIS AND NUMERICAL SOLUTION OF AN INTEGRAL EQUATION
METHOD FOR ELECTROMAGNETIC SCATTERING FROM A CAVITY IN A
GROUND PLANE

THESIS

Presented to the Faculty of the School of Engineering
of the Air Force Institute of Technology
Air University
In Partial Fulfillment of the
Requirements for the Degree of
Master of Science in Applied Mathematics

Eric T. Howe, B.A.,B.S.

September, 2001

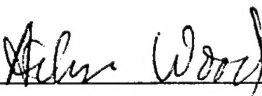
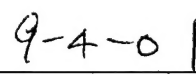
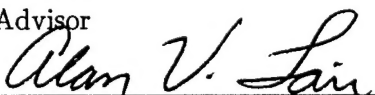
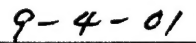
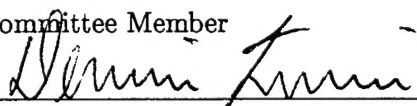
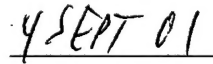
Approved for public release; distribution unlimited

AFIT/GAM/ENC/01S-1

ANALYSIS AND NUMERICAL SOLUTION OF AN INTEGRAL EQUATION
METHOD FOR ELECTROMAGNETIC SCATTERING FROM A CAVITY IN A
GROUND PLANE

Eric T. Howe, B.A.,B.S.

Approved:

	
Dr. Aihua Wood Thesis Advisor	Date
	
Dr. Alan Lair Committee Member	Date
	
Dr. Dennis Quinn Committee Member	Date

Acknowledgements

I would like to express my sincere gratitude to those who have assisted me in this research effort. My advisor, Dr. Aihua Wood, was great to work with and provided me with helpful guidance and insight. I also owe thanks to the members of my research committee, Dr. Alan Lair and Dr. Dennis Quinn, who gave much needed advice and encouragement throughout the project.

I would also like to thank Major William D. Wood whose dissertation work provided the basis for this research. Furthermore, I owe a tremendous debt of gratitude to Dr. Tri Van for all of the assistance he provided and for the many helpful conversations he had with me.

Finally, I would like to thank my family for their support during this difficult time as well as all of the friends I have made at AFIT. They have helped make the time spent here very enjoyable.

Eric T. Howe

Table of Contents

	Page
Acknowledgements	iii
List of Figures	vi
Abstract	viii
 I. Introduction	 1
1.1 Motivation	1
1.2 Organization	2
1.3 Related Work	3
 II. Theoretical Background	 5
2.1 Cavity Geometry	5
2.2 Problem Statement	6
2.3 Field Conditions	7
2.4 Green's Functions	9
 III. Integral Equation Theory	 11
3.1 Fundamental Theorems	11
3.2 Applications of the Fundamental Theorems	12
3.3 Derivation of Scalar Integral Equations	16
3.3.1 Scalar Equation 1	18
3.3.2 Scalar Equation 2	20
3.3.3 Scalar Equation 3	21
 IV. Numerical Solution	 23
4.1 Method of Moments	23
4.2 Cavity Discretization	26

	Page
4.3 Method of Moments Algorithm	26
4.3.1 Solution Scheme for Equation 1	27
4.3.2 Solution Scheme for Equation 2	30
4.3.3 Solution Scheme for Equation 3	31
4.4 Computing the Impedance Matrix	32
4.4.1 Computing A_1	34
4.4.2 Computing A_2	37
4.4.3 Computing A_3	41
4.5 Error Estimate	43
V. Numerical Results	45
5.1 Computing the Monostatic RCS	45
5.2 RCS Plots	48
5.2.1 Test Cavity 1	48
5.2.2 Test Cavity 2	54
5.2.3 Test Cavity 3	56
5.2.4 Test Cavity 4	58
5.2.5 Test Cavity 5	60
5.3 Error History Plots	62
VI. Conclusions	66
Bibliography	68

List of Figures

Figure		Page
1.	Cavity Geometry	5
2.	Incident and Scattered Fields	6
3.	Cavity Discretization	26
4.	Geometry of $\vec{\rho}'$	46
5.	Geometry of unfilled rectangular cavity	49
6.	Magnitude of the total magnetic field on the aperture, normal incidence	50
7.	Magnitude of the total magnetic field on the cavity surface, normal incidence	51
8.	Magnitude of the normal derivative of the magnetic field on the aperture, normal incidence	52
9.	Monostatic RCS signature of an unfilled rectangular cavity. Integral equation method (o) and RAM2D (—)	53
10.	Geometry of a deep rectangular cavity	54
11.	Monostatic RCS signature of a deep unfilled rectangular cavity. Integral equation method (o) and RAM2D (—)	55
12.	Geometry of a rectangular cavity filled with a lossy material	56
13.	Monostatic RCS signature of a rectangular cavity filled with a lossy dielectric material. Integral equation method (o) and finite element method (—)	57
14.	Geometry of a deep rectangular cavity filled with a lossy material .	58
15.	Monostatic RCS signature of a deep rectangular cavity filled with a dielectric material. Integral equation method (o) and finite element method (—)	59
16.	Geometry of a triangular cavity filled with a lossy material	60
17.	Monostatic RCS signature of a triangular cavity filled with a dielectric material. Integral equation method (o) and finite element method (—)	61
18.	Relative error history of an empty rectangular cavity for normal incidence	62

Figure		Page
19.	Log-Log plot of relative error history for normal incidence	63
20.	Relative error history of an empty rectangular cavity, $\theta = 10^\circ$. . .	63
21.	Log-Log plot of relative error history, $\theta = 10^\circ$	64
22.	Relative error history of a filled triangular cavity, $\theta = 35^\circ$	64
23.	Log-Log plot of relative error for a filled triangular cavity, $\theta = 35^\circ$.	65

Abstract

In this research the electromagnetic scattering of a plane wave from a two-dimensional cavity embedded in an infinite, perfectly conducting ground plane is investigated. The plane wave is assumed to be under transverse electric (TE) polarization with respect to the x -axis. The cavity may be empty or filled with an arbitrary homogeneous, lossy material. A coupled set of scalar integral equations that govern the electromagnetic scattering is implemented.

An approximate solution to the scalar integral equations is found via a Method of Moments (MoM) algorithm. The algorithm is implemented in a computer code, and approximations to the total magnetic field on the cavity surface and aperture as well as the normal derivative of the total magnetic field on the cavity aperture are obtained. These fields are then used to calculate the two-dimensional monostatic RCS signatures of various test cavities.

The numerical results from the algorithm are shown to agree well with the RCS signatures calculated by other well-known methods and published results. In addition to being accurate, the algorithm is very computationally efficient. The process results in simply solving a relatively small, well-conditioned matrix system for each incident angle to produce the unknown fields. Analytical and numerical error analysis shows the method to have approximately $\mathcal{O}(h)$ order of convergence, where h is an indication of the fineness of the mesh used to discretize the cavity.

ANALYSIS AND NUMERICAL SOLUTION OF AN INTEGRAL EQUATION METHOD FOR ELECTROMAGNETIC SCATTERING FROM A CAVITY IN A GROUND PLANE

I. Introduction

1.1 Motivation

The study of electromagnetic plane wave scattering and the measurement of the radar cross section (RCS) of targets has been of much interest in recent years to the military aircraft industry. Many practical applications arise which require knowledge of the RCS signature of a target. The RCS of a target is essentially a measure of the detectability of the target by a radar system. More rigorously, in three dimensions, the RCS or *echo area* is defined as the area intercepting the amount of power that, when scattered isotropically, produces at the receiver a density that is equal to the density scattered by the actual target [6]. In two dimensions the RCS parameter is referred to as the *echo width* or alternatively as the *radar cross section per unit length* of the target.

The accurate prediction and calculation of the RCS signature of targets is vitally important to today's military. The ability to control the RCS signatures of friendly air vehicles as well as the ability to detect and identify enemy air vehicles are both significant determining factors in the outcome of an air campaign. The camouflage of stealthy aircraft is one example of the need to minimize a friendly target's RCS signature. Stealth aircraft have proven to be a highly effective means of utilizing the element of surprise in an attack while providing increased survivability for American pilots, as evidenced by their success in the Persian Gulf War.

It may also be desirable in certain instances to be able to enhance the RCS signature of a friendly air vehicle. For example, the use of unmanned, remotely-piloted air vehicles to gather reconnaissance information and/or serve as decoys to confuse enemy defenses may be a very effective technique in certain tactical scenarios. Such a vehicle would

typically be much smaller than a fighter-size aircraft and consequently would have a smaller RCS signature. The ability to enhance the RCS signature of a smaller unmanned air vehicle, thereby reducing an enemy's capacity for distinguishing between it and a fighter-size aircraft, may be advantageous.

In either situation, whether reducing the RCS or enhancing the RCS of a target, it is necessary to have efficient methods of calculating the RCS signature of a scattering body. Complex objects such as military aircraft have many different design factors that can contribute to their RCS signature, but of particular interest is the prediction of the RCS patterns of cavities on the target's body. Cavities on an aircraft can include jet engine inlet ducts and exhaust nozzles, cavity-backed antennas, as well as cracks and gaps in the metallic body of the aircraft. Cavities are of such importance because the RCS of a cavity can potentially dominate the total RCS signature of an aircraft, and because the accurate prediction of cavity RCS can be very computationally challenging. Indeed, there is a wealth of mathematical and engineering literature on the design and analysis of electromagnetic cavities. (See, for example [1], [2], [3], [11], [16], and [24].) It would be far too expensive and time consuming to rely solely on real world measurements in the study of RCS reduction and enhancement, so accurate mathematical models and efficient computational algorithms capable of predicting RCS patterns are much desired.

1.2 Organization

The goal of this research is to develop an efficient and accurate method of calculating the scattered fields of an incident plane wave impinging on an open cavity embedded in a ground plane. These scattered fields can then be used to determine the RCS of the cavity. To accomplish this goal, a set of coupled integral equations (developed in [26]) are implemented and solved. In Chapter II, the cavity geometry and the problem statement are discussed as well as the fundamental concepts from electromagnetics and the conditions satisfied by all of the fields in the problem. Chapter III contains the development of the vector integral equations that govern the electromagnetic scattering of a plane wave from a cavity. The vector integral equations are then converted to a set of scalar integral equations.

Chapter IV contains a brief introduction to the general Method of Moments (MoM) procedure along with the approximate solution of the scalar integral equations through the development of a MoM algorithm. Chapter IV also contains an explanation of how certain singular integrals arise from the theory and how they can be treated so that they evaluate numerically. An estimate of the order of convergence of the MoM algorithm is also presented in this chapter. The numerical results are presented in Chapter V, including plots of the fields along the cavity aperture and cavity surface, plots of the monostatic RCS signatures of several test cavities, and relative error plots of the method. Chapter VI contains a summary of the results found along with recommendations for future research.

1.3 Related Work

The problem of predicting the electromagnetic scattering from a cavity in a ground plane has been fairly well studied, and there are many different techniques and approaches to solving the problem. As expected, these techniques have their advantages as well as their disadvantages. Some are more computationally efficient than others, while some provide more stable and accurate solutions. Presented here is a very brief overview of some of the more popular methods.

The generalized network formulation (GNF) was developed by Harrington and Mautz in 1976 to calculate the scattering from an open, perfectly conducting cavity in free space [14]. Their method partitions the cavity problem into two “simpler” problems, the exterior cavity problem and the interior cavity problem. Each of the two simpler problems is treated individually using equivalence relationships, then the composite problem is solved by enforcing the continuity of the tangential fields across the aperture of the cavity. The primary drawback to the GNF method is that the fields are not uniquely determinable at a countably infinite set of discrete, resonant frequencies [21]. At such frequencies a spurious, nonsensical solution is produced by the method. And since it is extremely difficult to determine the resonant frequencies of an arbitrarily shaped cavity, this is a rather significant drawback. Despite this hindrance, however, the GNF method has served as a springboard for many other methods. In fact, most integral equation approaches employ some form of a GNF implementation.

Other popular techniques used to solve the scattering problem have included the finite element method or the more popular hybrid finite element methods. These hybrid methods often combine traditional finite elements with boundary integral equations to solve the scattering problem from a cavity in a ground plane [18]. They have the advantage of being able to model cavities filled with arbitrary, inhomogeneous materials since the entire cavity interior is discretized with finite elements. Also, the spurious resonance problem discussed earlier can be avoided by introducing penalty functions to the equations [22]. However, the methods are typically more computationally burdensome due to the required meshing of the entire cavity interior and exterior. But this is admittedly becoming less and less of a problem as the performance of computers and the ease of the storage of information are dramatically improving.

Integral equation methods represent another very popular family of techniques for solving the cavity scattering problem. The electric field integral equation (EFIE) and magnetic field integral equation (MFIE) methods are easy to implement, but typically only work well for simple geometries. As mentioned earlier, since most integral equation methods are based on the GNF, they suffer from the problem of spurious resonances. However, a new integral equation method was introduced by Asvestas and Kleinman [4] in 1994. They developed a set of coupled vector integral equations for a three-dimensional unfilled cavity-backed aperture in a perfectly conducting ground plane, which were purportedly uniquely solvable at all frequencies. In his dissertation, Wood extended Asvestas and Kleinman's coupled vector integral equations to be able to account for material filled cavities [26]. The method he developed can be applied to electrically large and electrically small cavities, and it will not suffer from the problem of spurious resonances. Also, the technique requires solving only for the unknown fields along the cavity surface and aperture, so it is very computationally efficient. Based on the work presented in his dissertation, Wood and Wood developed a related set of scalar integral equations for the scattering from a material filled two-dimensional cavity in a ground plane of an electromagnetic wave under transverse magnetic (TM) polarization [27]. This current research effort focuses on the complement of this problem, considering an incident field under transverse electric (TE) polarization.

II. Theoretical Background

In this chapter, the general geometry of the embedded cavity is presented along with the formal problem statement. Some fundamental electromagnetic theory is then given, followed by the conditions that must be satisfied by all of the fields in the scattering problem. Finally, the Green's functions and dyadic functions necessary for the solution of the problem are defined.

2.1 Cavity Geometry

Consider the geometry of the two-dimensional cavity shown in Figure 1. The aperture, or cavity opening, is denoted as σ , and the surface of the cavity is called S . The interior of the cavity is denoted as D with boundary $\partial D = \sigma \cup S$ and outward pointing unit normal vector \hat{n} . The normal vector \hat{n} is defined almost everywhere, that is it is defined all along ∂D except for a finite number of edges, corners, or tips. The ground plane and the surface of the cavity are perfect electric conductors (PEC), and the upper half plane is free space with electric permittivity ϵ_0 and magnetic permeability μ_0 . The interior of the cavity D may either be empty or filled with a homogeneous material having permittivity ϵ_1 and permeability μ_1 . The complement of σ in the ground plane is called σ^c .

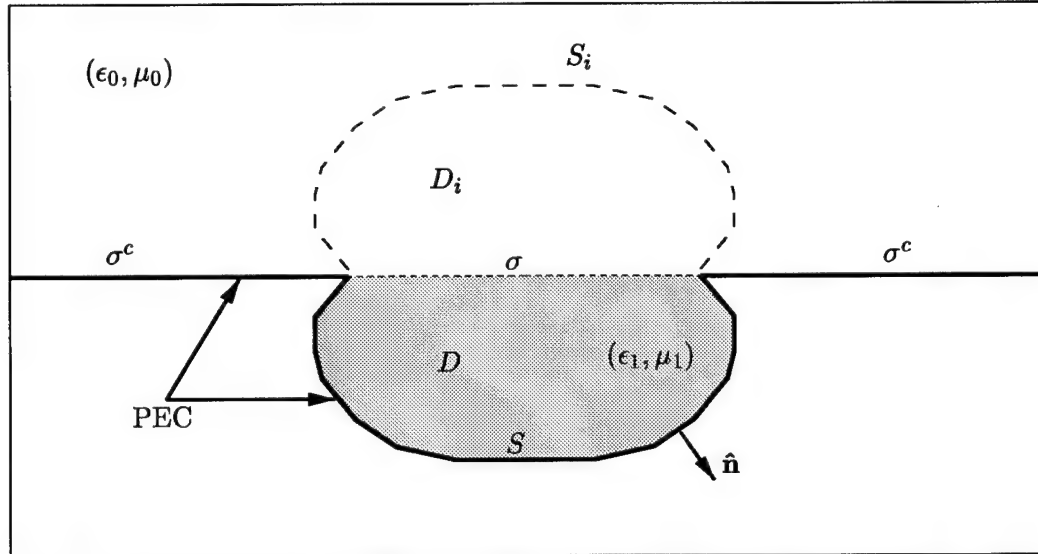


Figure 1 Cavity Geometry

The symbol \vec{r} will be used as a position vector, that is $\vec{r} = x\hat{x} + y\hat{y} + z\hat{z}$ in three dimensions. For the two-dimensional problem, the projection of the position vector into the yz -plane is used. It is of the form $\vec{\rho} = \vec{r} \cdot (\hat{y}\hat{y} + \hat{z}\hat{z}) = y\hat{y} + z\hat{z}$. The image of an object will be defined as the reflection of the object across the ground plane or aperture. For example, the images of S and D in Figure 1 are S_i and D_i , respectively. The image of a point given by $\vec{\rho} = y\hat{y} + z\hat{z}$ is the point $\vec{\rho}_i = \vec{\rho} \cdot \bar{\bar{\mathbf{I}}}_i = y\hat{y} - z\hat{z}$, where $\bar{\bar{\mathbf{I}}}_i = \hat{y}\hat{y} - \hat{z}\hat{z}$ is the image dyadic. The image of an object will always be denoted with the subscript i after it. Similarly, a field vector function is defined to be $\vec{\mathbf{A}}(\vec{r}) = A_x(\vec{r})\hat{x} + A_y(\vec{r})\hat{y} + A_z(\vec{r})\hat{z}$, and its image is defined as $\vec{\mathbf{A}}_i(\vec{r}) = A_x(\vec{r})\hat{x} + A_y(\vec{r})\hat{y} - A_z(\vec{r})\hat{z}$.

2.2 Problem Statement

In the problem considered, a known incident plane wave whose electric and magnetic fields are represented by $(\vec{\mathbf{E}}^{\text{inc}}, \vec{\mathbf{H}}^{\text{inc}})$ impinges on the cavity giving rise to the unknown scattered electric and magnetic fields $(\vec{\mathbf{E}}^{\text{s}}, \vec{\mathbf{H}}^{\text{s}})$ as shown in Figure 2. The incident plane wave propagates at an incident angle $0 < \theta < \pi$ with respect to the positive y -axis. Under transverse electric (TE) polarization, the magnetic field of the incident plane wave is parallel to the longitudinal x -axis, that is $\vec{\mathbf{H}}^{\text{inc}} = (u^{\text{inc}}, 0, 0)$. The electric field of the incident wave has both a y - and a z -component.

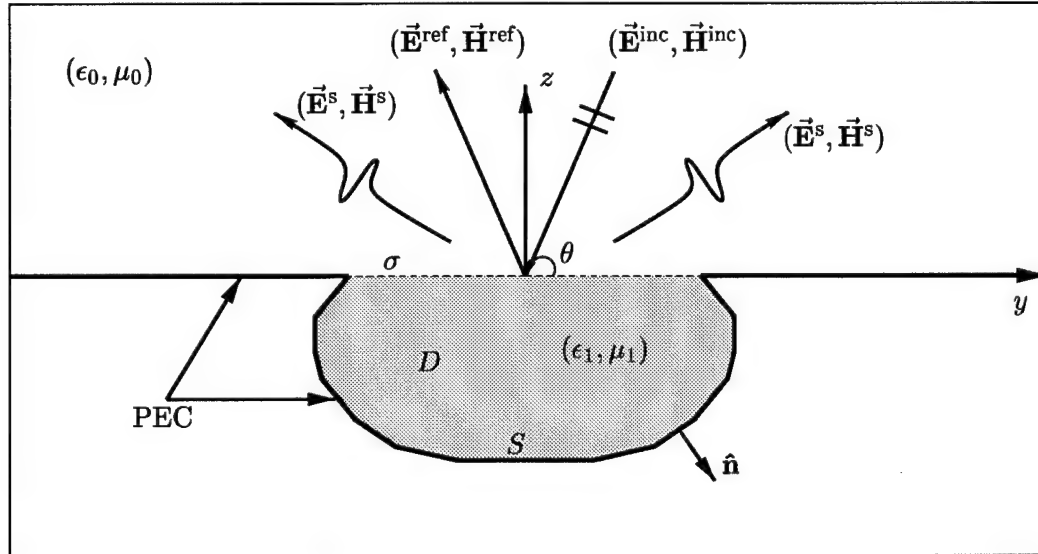


Figure 2 Incident and Scattered Fields

The given incident fields are defined to be those fields that exist in unbounded free space. The scattered fields are those that are caused by the presence of the scatterer, in this case the embedded cavity. They are defined in terms of the total field and the reflected field as $\vec{\mathbf{E}}^s = \vec{\mathbf{E}} - \vec{\mathbf{E}}^{\text{inc}} - \vec{\mathbf{E}}^{\text{ref}}$ and $\vec{\mathbf{H}}^s = \vec{\mathbf{H}} - \vec{\mathbf{H}}^{\text{inc}} - \vec{\mathbf{H}}^{\text{ref}}$, where $\vec{\mathbf{E}} \equiv \vec{\mathbf{E}}(\vec{\mathbf{r}})$ is the total electric field intensity in the region in volts per meter, and $\vec{\mathbf{H}} \equiv \vec{\mathbf{H}}(\vec{\mathbf{r}})$ is the total magnetic field intensity in the region in Amperes per meter. The reflected fields $\vec{\mathbf{E}}^{\text{ref}}$ and $\vec{\mathbf{H}}^{\text{ref}}$ are defined to be those scattered by an unbroken, PEC ground plane located at $z = 0$.

2.3 Field Conditions

The upper half plane and the interior of the cavity are restricted to be source free so that the only source introduced will be the incident plane wave. Therefore, the total fields in D and its reflection in the upper half plane D_i satisfy the following Maxwell's equations for homogeneous, linear, isotropic, source-free media. Using the $e^{j\omega t}$ time convention, these equations are given as

$$\nabla \times \vec{\mathbf{E}} = -j\omega\mu\vec{\mathbf{H}} \quad (1)$$

$$\nabla \times \vec{\mathbf{H}} = j\omega\epsilon\vec{\mathbf{E}} \quad (2)$$

$$\nabla \cdot \vec{\mathbf{E}} = 0 \quad (3)$$

$$\nabla \cdot \vec{\mathbf{H}} = 0 \quad (4)$$

where ω is the radian frequency (radians/second), μ is the magnetic permeability of the medium (Henrys/meter), ϵ is the electric permittivity of the medium (Farads/meter), and $j = \sqrt{-1}$ is the imaginary unit [6]. Taking the curl of equations (1) and (2) and substituting in appropriate terms reveals that both $\vec{\mathbf{E}}$ and $\vec{\mathbf{H}}$ satisfy the homogeneous wave equation

$$\nabla \times \nabla \times \vec{\mathbf{E}}(\vec{\mathbf{r}}) - k^2\vec{\mathbf{E}}(\vec{\mathbf{r}}) = 0 \quad (5)$$

$$\nabla \times \nabla \times \vec{\mathbf{H}}(\vec{\mathbf{r}}) - k^2\vec{\mathbf{H}}(\vec{\mathbf{r}}) = 0 \quad (6)$$

where $k = \omega\sqrt{\mu\epsilon}$ is the propagation constant or *wave number* of the medium in inverse meters.

In addition to satisfying Maxwell's equations for a source-free region, the total fields must also satisfy certain boundary conditions. Since the ground plane and the surface of the cavity S are perfect electric conductors, the tangential component of the total electric field will be "shorted out" there. So the electric field must satisfy the boundary conditions

$$\hat{\mathbf{n}} \times \vec{\mathbf{E}}(\vec{\mathbf{r}}) = 0 \quad \text{for } \vec{\mathbf{r}} \in S \quad (7)$$

$$\hat{\mathbf{z}} \times \vec{\mathbf{E}}(\vec{\mathbf{r}}) = 0 \quad \text{for } \vec{\mathbf{r}} \in \sigma^c \quad (8)$$

where σ^c is the complement of the aperture in the ground plane (i.e. the part of the ground plane that is undisturbed by the presence of the cavity). Furthermore, the tangential components of the total electric field and the total magnetic field must be continuous across the aperture σ . This can be written as

$$\lim_{\delta \rightarrow 0} \left[\hat{\mathbf{z}} \times \vec{\mathbf{E}}(\vec{\mathbf{r}} + \delta \hat{\mathbf{z}}) - \hat{\mathbf{z}} \times \vec{\mathbf{E}}(\vec{\mathbf{r}} - \delta \hat{\mathbf{z}}) \right] = 0 \quad \text{for } \vec{\mathbf{r}} \in \sigma \quad (9)$$

$$\lim_{\delta \rightarrow 0} \left[\hat{\mathbf{z}} \times \vec{\mathbf{H}}(\vec{\mathbf{r}} + \delta \hat{\mathbf{z}}) - \hat{\mathbf{z}} \times \vec{\mathbf{H}}(\vec{\mathbf{r}} - \delta \hat{\mathbf{z}}) \right] = 0 \quad \text{for } \vec{\mathbf{r}} \in \sigma \quad (10)$$

The final field conditions that must be satisfied pertain to the scattered fields. Specifically, the Sommerfeld radiation conditions must be satisfied at infinity

$$\lim_{|\vec{\mathbf{r}}| \rightarrow \infty} \left[\vec{\mathbf{r}} \cdot \nabla \vec{\mathbf{E}}^s(\vec{\mathbf{r}}) + jk|\vec{\mathbf{r}}| \vec{\mathbf{E}}^s(\vec{\mathbf{r}}) \right] = 0 \quad (11)$$

$$\lim_{|\vec{\mathbf{r}}| \rightarrow \infty} \left[\vec{\mathbf{r}} \cdot \nabla \vec{\mathbf{H}}^s(\vec{\mathbf{r}}) + jk|\vec{\mathbf{r}}| \vec{\mathbf{H}}^s(\vec{\mathbf{r}}) \right] = 0 \quad (12)$$

as well as the regularity conditions [26]:

$$\lim_{|\vec{\mathbf{r}}| \rightarrow \infty} |\vec{\mathbf{r}}| \vec{\mathbf{E}}^s(\vec{\mathbf{r}}) = 0 \quad (13)$$

$$\lim_{|\vec{\mathbf{r}}| \rightarrow \infty} |\vec{\mathbf{r}}| \vec{\mathbf{H}}^s(\vec{\mathbf{r}}) = 0 \quad (14)$$

2.4 Green's Functions

The three-dimensional scalar Green's function commonly associated with electromagnetic radiation and scattering problems is defined as

$$G(k; \vec{r}, \vec{r}') = \frac{e^{-jkR}}{4\pi R} \quad (15)$$

$$R = |\vec{r} - \vec{r}'|$$

where $\vec{r} = x\hat{x} + y\hat{y} + z\hat{z}$ and $\vec{r}' = x'\hat{x} + y'\hat{y} + z'\hat{z}$ are position vectors in unprimed and primed coordinates, respectively. (This will be converted to the two-dimensional case and applied to the current problem later in the thesis.) In [26], the Green's function in equation (15) was shown to satisfy the distributional differential equation

$$\nabla^2 G + k^2 G = -\delta(\vec{r} - \vec{r}') \quad (16)$$

where δ is the Dirac delta distribution. The Green's function also satisfies the scalar analogues of the radiation and regularity conditions given in the previous section.

Define the auxiliary scalar functions

$$G_D(k; \vec{r}, \vec{r}') = G(k; \vec{r}, \vec{r}') - G(k; \vec{r}, \vec{r}'_i) \quad (17)$$

$$G_N(k; \vec{r}, \vec{r}') = G(k; \vec{r}, \vec{r}') + G(k; \vec{r}, \vec{r}'_i) \quad (18)$$

as linear combinations of the scalar Green's function in equation (15) with different arguments. The function G_D is referred to as the Dirichlet scalar half-space Green's function, and G_N as the Neumann scalar half-space Green's function. Next, define the dyadic function

$$\bar{\bar{\Gamma}}(k; \vec{r}, \vec{r}') = -jk \nabla G(k; \vec{r}, \vec{r}') \times \bar{\bar{\mathbf{I}}} \quad (19)$$

where $\bar{\bar{\mathbf{I}}} = \hat{x}\hat{x} + \hat{y}\hat{y} + \hat{z}\hat{z}$ is called the idemfactor.

Finally, define the auxiliary dyadic functions

$$\bar{\bar{\Gamma}}_1 = -jk \left(\nabla G_N \times \bar{\bar{\mathbf{I}}}_t + \nabla G_D \times \hat{z}\hat{z} \right) \quad (20)$$

and

$$\bar{\bar{\Gamma}}_2 = -jk \left(\nabla G_D \times \bar{\bar{\mathbf{I}}}_t + \nabla G_N \times \hat{\mathbf{z}}\hat{\mathbf{z}} \right), \quad (21)$$

where $\bar{\bar{\mathbf{I}}}_t = \hat{\mathbf{x}}\hat{\mathbf{x}} + \hat{\mathbf{y}}\hat{\mathbf{y}}$ is called the transverse idemfactor. It can be shown that the auxiliary dyadic functions in equations (20) and (21) satisfy the homogeneous boundary conditions

$$\hat{\mathbf{z}} \times \bar{\bar{\Gamma}}_1 = 0 \quad \text{for } z = 0 \quad (22)$$

$$\hat{\mathbf{z}} \times \nabla \times \bar{\bar{\Gamma}}_2 = 0 \quad \text{for } z = 0 \quad (23)$$

as well as the equations

$$\hat{\mathbf{z}} \cdot \left[\vec{\mathbf{A}}(\vec{\mathbf{r}}) \times \nabla \times \bar{\bar{\Gamma}}_1(k; \vec{\mathbf{r}}, \vec{\mathbf{r}}') \right] = 2\hat{\mathbf{z}} \cdot \left[\vec{\mathbf{A}}(\vec{\mathbf{r}}) \times \nabla \times \bar{\bar{\Gamma}}(k; \vec{\mathbf{r}}, \vec{\mathbf{r}}') \right] \quad \text{for } z = 0 \quad (24)$$

$$\hat{\mathbf{z}} \cdot \left[\vec{\mathbf{A}}(\vec{\mathbf{r}}) \times \bar{\bar{\Gamma}}_2(k; \vec{\mathbf{r}}, \vec{\mathbf{r}}') \right] = 2\hat{\mathbf{z}} \cdot \left[\vec{\mathbf{A}}(\vec{\mathbf{r}}) \times \bar{\bar{\Gamma}}(k; \vec{\mathbf{r}}, \vec{\mathbf{r}}') \right] \quad \text{for } z = 0 \quad (25)$$

The scalar and dyadic functions presented in this section were first introduced in [4], and then in [26]. They are the fundamental building blocks in the development of the coupled vector integral equations for the scattering problem which are presented in the next chapter.

III. Integral Equation Theory

In this chapter, the fundamental theorems and the coupled set of vector integral equations developed by Asvestas and Kleinman in [4] and extended by Wood in [26] are presented. The set of vector integral equations is converted to a set of scalar integral equations for the two-dimensional scattering problem under TE polarization which will be solved approximately by a Method of Moments algorithm.

3.1 Fundamental Theorems

All of the theorems presented in this section first appeared in [4] and were later extended in [26]. The proof of the theorems can be found in [26]. The theorems are as follows.

Theorem 1 *Let V be a homogeneous region with regular boundary ∂V , $\hat{\mathbf{n}}$ be the outward unit normal vector on ∂V , and $\bar{\bar{\Gamma}} \equiv \bar{\bar{\Gamma}}(k; \vec{\mathbf{r}}, \vec{\mathbf{r}}')$ be defined as in equation (19). If $\vec{\mathbf{A}} \equiv \vec{\mathbf{A}}(\vec{\mathbf{r}})$ satisfies $\nabla \times \nabla \times \vec{\mathbf{A}} - k^2 \vec{\mathbf{A}} = \vec{\mathbf{0}} \quad \forall \quad \vec{\mathbf{r}} \in V$, then*

$$\int_{\partial V} \hat{\mathbf{n}} \cdot [\vec{\mathbf{A}} \times (\nabla \times \bar{\bar{\Gamma}}) + (\nabla \times \vec{\mathbf{A}}) \times \bar{\bar{\Gamma}}] ds = \begin{cases} jk \nabla' \times \vec{\mathbf{A}}(\vec{\mathbf{r}}') & \vec{\mathbf{r}}' \in V \\ 0 & \vec{\mathbf{r}}' \notin \bar{V} \end{cases} \quad (26)$$

where \bar{V} is the closure of V ; that is, the union of V and its boundary.

Theorem 2 *Let V , \bar{V} , ∂V , $\hat{\mathbf{n}}$, and $\vec{\mathbf{A}}$ be defined as in Theorem 1. Let $\bar{\bar{\Gamma}}_1$ be defined by equation (20), V_i be the image of V with respect to the xy -plane, and \bar{V}_i be the closure of V_i . Then*

$$\int_{\partial V} \hat{\mathbf{n}} \cdot [\vec{\mathbf{A}} \times (\nabla \times \bar{\bar{\Gamma}}_1) + (\nabla \times \vec{\mathbf{A}}) \times \bar{\bar{\Gamma}}_1] ds = \begin{cases} jk \nabla' \times \vec{\mathbf{A}}(\vec{\mathbf{r}}') & \vec{\mathbf{r}}' \in V \\ jk [\nabla'_i \times \vec{\mathbf{A}}(\vec{\mathbf{r}}'_i)]_i & \vec{\mathbf{r}}' \in V_i \\ 0 & \vec{\mathbf{r}}' \notin \bar{V} \cup \bar{V}_i \end{cases} \quad (27)$$

Theorem 3 Let V , \bar{V} , ∂V , V_i , \bar{V}_i , $\hat{\mathbf{n}}$, and $\vec{\mathbf{A}}$ be defined as in Theorem 2. Let $\bar{\bar{\Gamma}}_2$ be defined by equation (21). Then

$$\int_{\partial V} \hat{\mathbf{n}} \cdot \left[\vec{\mathbf{A}} \times (\nabla \times \bar{\bar{\Gamma}}_2) + (\nabla \times \vec{\mathbf{A}}) \times \bar{\bar{\Gamma}}_2 \right] ds = \begin{cases} jk \nabla' \times \vec{\mathbf{A}}(\vec{\mathbf{r}}') & \vec{\mathbf{r}}' \in V \\ -jk \left[\nabla'_i \times \vec{\mathbf{A}}(\vec{\mathbf{r}}'_i) \right]_i & \vec{\mathbf{r}}' \in V_i \\ 0 & \vec{\mathbf{r}}' \notin \bar{V} \cup \bar{V}_i \end{cases} \quad (28)$$

In the preceding theorems, the del operator ∇ differentiates with respect to unprimed coordinates, while ∇' differentiates with respect to primed coordinates. Also, the operator ∇'_i is the same as ∇' except that $\frac{\partial}{\partial z'}$ is replaced by $\frac{-\partial}{\partial z'}$. It is pointed out in both [4] and [26] that the theorems do not hold when $\vec{\mathbf{r}}'$ lies exactly on the region's boundary ∂V , but that they are valid as $\vec{\mathbf{r}}'$ approaches ∂V from either the interior or the exterior of V .

The theorems relate a vector function evaluated at a point to an integral over a closed surface. Also, notice that they are stated in very general terms. The only requirements are that the vector function $\vec{\mathbf{A}}(\vec{\mathbf{r}})$ satisfy the homogeneous wave equation and that the outward pointing unit normal vector $\hat{\mathbf{n}}$ be defined almost everywhere on ∂V .

3.2 Applications of the Fundamental Theorems

The theorems presented in the previous section can now be applied to the embedded cavity scattering problem. This is accomplished by associating V with either the cavity volume D or the upper half space, $z > 0$, and by letting $\vec{\mathbf{A}}(\vec{\mathbf{r}})$ take on the various field components of the cavity scattering problem.

Application 1 Let $V = D$, $\vec{\mathbf{A}} = \vec{\mathbf{H}}$, and $\vec{\mathbf{r}}' \in D$ in Theorem 1. By applying Maxwell's equation (2) and the boundary condition in equation (7), Theorem 1 can be rewritten as

$$\begin{aligned} k_1^2 Y_1 \vec{\mathbf{E}}(\vec{\mathbf{r}}') &= - \int_{\partial D} \left(\hat{\mathbf{n}} \times \vec{\mathbf{H}}(\vec{\mathbf{r}}) \right) \cdot \nabla \times \bar{\bar{\Gamma}}(k_1; \vec{\mathbf{r}}, \vec{\mathbf{r}}') ds \\ &\quad - jk_1 Y_1 \int_{\sigma} \left(\hat{\mathbf{z}} \times \vec{\mathbf{E}}(\vec{\mathbf{r}}) \right) \cdot \bar{\bar{\Gamma}}(k_1; \vec{\mathbf{r}}, \vec{\mathbf{r}}') d\sigma. \end{aligned} \quad (29)$$

In equation (29), $Y_1 = \sqrt{\epsilon_1/\mu_1}$ is the intrinsic admittance of the cavity material. This application shows that the total electric field at any point in the cavity volume is a function of the tangential electric and magnetic fields on the cavity surface and aperture.

Application 2 Let $V = D$, $\vec{\mathbf{A}} = \vec{\mathbf{E}}$, and $\vec{\mathbf{r}}' \in D$ in Theorem 1. By applying Maxwell's equation (1) and the boundary condition in equation (7), Theorem 1 can be rewritten as

$$\begin{aligned} k_1^2 Z_1 \vec{\mathbf{H}}(\vec{\mathbf{r}}') &= \int_{\sigma} \left(\hat{\mathbf{z}} \times \vec{\mathbf{E}}(\vec{\mathbf{r}}) \right) \cdot \nabla \times \bar{\bar{\Gamma}}(k_1; \vec{\mathbf{r}}, \vec{\mathbf{r}}') d\sigma \\ &\quad - j k_1 Z_1 \int_S \left(\hat{\mathbf{n}} \times \vec{\mathbf{H}}(\vec{\mathbf{r}}) \right) \cdot \bar{\bar{\Gamma}}(k_1; \vec{\mathbf{r}}, \vec{\mathbf{r}}') ds \end{aligned} \quad (30)$$

where $Z_1 = \sqrt{\mu_1/\epsilon_1}$ is the intrinsic impedance of the cavity material. This application demonstrates that the total magnetic field at any point in the cavity volume is a function of the tangential electric and magnetic fields on the cavity surface and aperture.

Application 3 Let V be the upper half space ($z > 0$), $\vec{\mathbf{A}} = \vec{\mathbf{E}}^s$, and $z' > 0$ in Theorem 2. By applying Maxwell's equation (1) and the conditions in equations (8), (22), and (24), Theorem 2 can be rewritten as

$$\frac{-k_0^2 Z_0}{2} \vec{\mathbf{H}}^s(\vec{\mathbf{r}}') = \int_{\sigma} \hat{\mathbf{z}} \times \vec{\mathbf{E}}(\vec{\mathbf{r}}) \cdot \nabla \times \bar{\bar{\Gamma}}(k_0; \vec{\mathbf{r}}, \vec{\mathbf{r}}') d\sigma. \quad (31)$$

According to the third application, the scattered magnetic field at any point in the upper half space is a function of the tangential electric field on the cavity aperture.

Application 4 Let $V = D$, $\vec{\mathbf{A}} = \vec{\mathbf{E}}$, and $\vec{\mathbf{r}}' \in D$ in Theorem 3. Using Maxwell's equation (1) and the conditions in equations (7), (23), and (25), Theorem 3 can be rewritten as

$$\begin{aligned} j k_1 \vec{\mathbf{H}}(\vec{\mathbf{r}}') &= 2 \int_{\sigma} \left(\hat{\mathbf{z}} \times \vec{\mathbf{H}}(\vec{\mathbf{r}}) \right) \cdot \bar{\bar{\Gamma}}(k_1; \vec{\mathbf{r}}, \vec{\mathbf{r}}') d\sigma \\ &\quad + \int_S \left(\hat{\mathbf{n}} \times \vec{\mathbf{H}}(\vec{\mathbf{r}}) \right) \cdot \bar{\bar{\Gamma}}_2(k_1; \vec{\mathbf{r}}, \vec{\mathbf{r}}') ds \end{aligned} \quad (32)$$

This application shows that the total magnetic field at any point in the cavity volume is a function of the tangential magnetic field on the cavity surface and aperture.

Application 5 Let V be the upper half space ($z > 0$), $\vec{\mathbf{A}} = \vec{\mathbf{H}}^s$, and $z' > 0$ in Theorem 3. By applying Maxwell's equation (2) and the conditions in equations (8), (23),

and (25), Theorem 3 can be rewritten as

$$\frac{-jk_0}{2}\vec{\mathbf{E}}^s(\vec{\mathbf{r}}') = \int_{\sigma} \hat{\mathbf{z}} \times \vec{\mathbf{E}}(\vec{\mathbf{r}}) \cdot \vec{\Gamma}(k_0; \vec{\mathbf{r}}, \vec{\mathbf{r}}') d\sigma. \quad (33)$$

According to this application, the scattered electric field at any point in the upper half space is a function of the tangential electric field on the cavity aperture. Equation (33) will be used later to determine the monostatic RCS values once the unknown tangential field components have been found.

The applications of the fundamental theorems define the total fields in the cavity volume and the scattered fields in the upper half space in terms of the tangential field components on the cavity surface S and the cavity aperture σ . So it is sufficient to find these tangential field components to solve the cavity scattering problem. Examining equations (29) through (33), it is apparent that there are two different types of field quantities involved. The left hand sides of equations (29)-(33) involve field quantities evaluated at points away from the boundary of the cavity ∂D , whereas the right hand sides of the equations involve the tangential components of the total fields evaluated on ∂D .

In order to make equations (29)-(32) more useful, consider letting $\vec{\mathbf{r}}'$ approach ∂D and then sifting out the tangential component of the result as suggested by Wood in [26]. Begin by fixing a point $\vec{\mathbf{r}}$ on ∂D so that $\hat{\mathbf{n}}$ is the outward unit normal vector at $\vec{\mathbf{r}}$, and then cross multiply the equations by $\hat{\mathbf{n}}$. Finally, let $\vec{\mathbf{r}}' = \vec{\mathbf{r}} + \delta\hat{\mathbf{n}}$ and evaluate the limit as $\delta \rightarrow 0$. Wood [26] also presents a theorem to help facilitate the limiting process.

Theorem 4 *Let V be a volume with regular boundary ∂V , $\vec{\mathbf{r}}$ be a fixed point on ∂V , $\hat{\mathbf{n}}$ be the outward unit normal vector at $\vec{\mathbf{r}}$, and $\vec{\Gamma}(k; \vec{\mathbf{r}}, \vec{\mathbf{r}}')$ be defined as in equation (19). If $\vec{\mathbf{A}}(\vec{\mathbf{r}})$ is continuous on ∂V , then*

$$\lim_{\vec{\mathbf{r}}' \rightarrow \vec{\mathbf{r}}} \hat{\mathbf{n}} \times \int_{\partial V} \vec{\mathbf{A}}(\vec{\mathbf{r}}'') \cdot \vec{\Gamma}(k; \vec{\mathbf{r}}'', \vec{\mathbf{r}}') ds'' = \mp \frac{jk}{2} \vec{\mathbf{A}}(\vec{\mathbf{r}}) + \hat{\mathbf{n}} \times \int_{\partial V} \vec{\mathbf{A}}(\vec{\mathbf{r}}'') \cdot \vec{\Gamma}(k; \vec{\mathbf{r}}'', \vec{\mathbf{r}}) ds'' \quad (34)$$

where the upper sign is taken if $\vec{\mathbf{r}}' \rightarrow \vec{\mathbf{r}}$ from the exterior of V , and the lower sign is taken if $\vec{\mathbf{r}}' \rightarrow \vec{\mathbf{r}}$ from the interior of V .

Application 1a Fix $\vec{r} \in \sigma$ so that $\hat{n} = \hat{z}$, and set $\vec{r}' = \vec{r} - \delta\hat{z}$, where $\delta > 0$. Cross multiplying equation (29) by \hat{z} and taking the limit as $\delta \rightarrow 0$ via Theorem 4 simplifies the equation to

$$\frac{-k_1^2 Y_1}{2} \hat{z} \times \vec{E}(\vec{r}') = \hat{z} \times \int_{\partial D} (\hat{n} \times \vec{H}(\vec{r})) \cdot \nabla \times \bar{\bar{\Gamma}}(k_1; \vec{r}, \vec{r}') ds \quad \text{for } \vec{r}' \in \sigma. \quad (35)$$

Notice that the second integral in equation (29) vanished in the limiting process. This is because $\hat{z} \times \left[(\hat{z} \times \vec{E}(\vec{r})) \cdot \bar{\bar{\Gamma}}(k_1; \vec{r}, \vec{r}') \right] = 0$ when $\vec{r} \in \sigma$ and $\vec{r}' \in \sigma$. This new application shows that the tangential electric field on the aperture σ can be expressed as a function of the tangential magnetic field on ∂D .

Application 2a Fix $\vec{r} \in \sigma$ so that $\hat{n} = \hat{z}$, and set $\vec{r}' = \vec{r} - \delta\hat{z}$, where $\delta > 0$. Again, cross multiplying equation (30) by \hat{z} and taking the limit as $\delta \rightarrow 0$ using Theorem 4, the equation can be written as

$$\begin{aligned} \frac{k_1^2 Z_1}{2} \hat{z} \times \vec{H}(\vec{r}') &= \hat{z} \times \int_{\sigma} (\hat{z} \times \vec{E}(\vec{r})) \cdot \nabla \times \bar{\bar{\Gamma}}(k_1; \vec{r}, \vec{r}') d\sigma \\ -jk_1 Z_1 \hat{z} \times \int_S (\hat{n} \times \vec{H}(\vec{r})) \cdot \bar{\bar{\Gamma}}(k_1; \vec{r}, \vec{r}') ds &\quad \text{for } \vec{r}' \in \sigma. \end{aligned} \quad (36)$$

This application now says that the tangential magnetic field on σ can be expressed as a function of the tangential magnetic field on S and the tangential electric field on σ .

Application 3a Fix $\vec{r} \in \sigma$ so that $\hat{n} = \hat{z}$, and set $\vec{r}' = \vec{r} + \delta\hat{z}$, where $\delta > 0$. Cross multiply equation (31) by \hat{z} and take the limit as $\delta \rightarrow 0$ using Theorem 4 to obtain

$$\frac{-k_0^2 Z_0}{2} \hat{z} \times \vec{H}^s(\vec{r}') = \hat{z} \times \int_{\sigma} \hat{z} \times \vec{E}(\vec{r}) \cdot \nabla \times \bar{\bar{\Gamma}}(k_0; \vec{r}, \vec{r}') d\sigma \quad \text{for } \vec{r}' \in \sigma. \quad (37)$$

Recall that $\vec{H}^s = \vec{H} - \vec{H}^{\text{inc}} - \vec{H}^{\text{ref}}$. Also note that along the aperture since $\hat{z} \times \vec{H}^{\text{inc}} = \hat{z} \times \vec{H}^{\text{ref}}$, equation (37) can be rewritten as

$$\begin{aligned} \frac{-k_0^2 Z_0}{2} \hat{z} \times [\vec{H}(\vec{r}') - 2\vec{H}^{\text{inc}}(\vec{r}')] &= \\ \hat{z} \times \int_{\sigma} \hat{z} \times \vec{E}(\vec{r}) \cdot \nabla \times \bar{\bar{\Gamma}}(k_0; \vec{r}, \vec{r}') d\sigma &\quad \text{for } \vec{r}' \in \sigma. \end{aligned} \quad (38)$$

Application 4a Fix $\vec{r} \in S$ and set $\vec{r}' = \vec{r} - \delta \hat{z}$, where $\delta > 0$. Cross multiply equation (32) by \hat{n}' and take the limit as $\delta \rightarrow 0$ using Theorem 4 to obtain

$$\begin{aligned} \frac{jk_1}{2} \hat{n}' \times \vec{H}(\vec{r}') &= 2\hat{n}' \times \int_{\sigma} \left(\hat{z} \times \vec{H}(\vec{r}) \right) \cdot \bar{\bar{\Gamma}}(k_1; \vec{r}, \vec{r}') d\sigma \\ &+ \hat{n}' \times \int_S \left(\hat{n} \times \vec{H}(\vec{r}) \right) \cdot \bar{\bar{\Gamma}}_2(k_1; \vec{r}, \vec{r}') ds \quad \text{for } \vec{r}' \in S. \end{aligned} \quad (39)$$

The equations in Applications 2a and 3a can be combined and simplified. Doing so results in a system of three coupled vector integral equations that govern the electromagnetic scattering from an embedded cavity in a perfectly conducting ground plane. Formally, the system of vector integral equations can be written as

$$\begin{aligned} \hat{z} \times \int_{\sigma} \left(\hat{z} \times \vec{H}(\vec{r}) \right) \cdot \nabla \times \bar{\bar{\Gamma}}(k_1; \vec{r}, \vec{r}') d\sigma + \hat{z} \times \int_S \left(\hat{n} \times \vec{H}(\vec{r}) \right) \cdot \nabla \times \bar{\bar{\Gamma}}(k_1; \vec{r}, \vec{r}') ds \\ = \frac{-k_1^2 Y_1}{2} \hat{z} \times \vec{E}(\vec{r}') \quad \text{for } \vec{r}' \in \sigma, \end{aligned} \quad (40)$$

$$\begin{aligned} -\hat{z} \times \int_{\sigma} \hat{z} \times \vec{E}(\vec{r}) \cdot \left\{ \frac{\nabla \times \bar{\bar{\Gamma}}(k_1; \vec{r}, \vec{r}')}{-jk_1} - \frac{\nabla \times \bar{\bar{\Gamma}}(k_0; \vec{r}, \vec{r}')}{-jk_0} \right\} d\sigma + \frac{jk_1 Z_1 + jk_0 Z_0}{2} \hat{z} \times \vec{H}(\vec{r}') \\ - Z_1 \hat{z} \times \int_S \hat{n} \times \vec{H}(\vec{r}) \cdot \bar{\bar{\Gamma}}(k_1; \vec{r}, \vec{r}') ds = jk_0 Z_0 \hat{z} \times \vec{H}^{\text{inc}}(\vec{r}') \quad \text{for } \vec{r}' \in \sigma, \end{aligned} \quad (41)$$

and

$$\begin{aligned} 2\hat{n}' \times \int_{\sigma} \left(\hat{z} \times \vec{H}(\vec{r}) \right) \cdot \bar{\bar{\Gamma}}(k_1; \vec{r}, \vec{r}') d\sigma + \hat{n}' \times \int_S \left(\hat{n} \times \vec{H}(\vec{r}) \right) \cdot \bar{\bar{\Gamma}}_2(k_1; \vec{r}, \vec{r}') ds \\ = \frac{jk_1}{2} \hat{n}' \times \vec{H}(\vec{r}') \quad \text{for } \vec{r}' \in S. \end{aligned} \quad (42)$$

3.3 Derivation of Scalar Integral Equations

In this section, the vector integral equations (40)-(42) are converted to a system of scalar integral equations for the scattering problem, where the incident plane wave is under transverse electric (TE) polarization. The derivation is similar to the method presented in [27] where scalar equations were developed for transverse magnetic (TM) polarization.

The necessary field quantities and unknowns are defined and then substituted into the vector equations. These are then simplified and converted to scalar equations which can be solved approximately by a Method of Moments (MoM) algorithm.

Under TE polarization, all of the components of the magnetic field are parallel to the longitudinal x -axis. For a plane wave, define the magnetic portion of the incident field to be

$$\vec{\mathbf{H}}^{\text{inc}}(y, z) = e^{jk_0(y \cos \theta + z \sin \theta)} \hat{\mathbf{x}} \quad (43)$$

and the unknown total magnetic field as

$$\vec{\mathbf{H}}(y, z) = u(y, z) \hat{\mathbf{x}} \quad (44)$$

where $u(y, z)$ is some unknown continuous function. Then applying Maxwell's equations, the corresponding incident and total electric fields can be shown to be

$$\vec{\mathbf{E}}^{\text{inc}}(y, z) = Z_0(\sin \theta \hat{\mathbf{y}} - \cos \theta \hat{\mathbf{z}}) e^{jk_0(y \sin \theta + z \cos \theta)} \quad (45)$$

and

$$\vec{\mathbf{E}}(y, z) = \frac{1}{j\omega\epsilon_1} \nabla u \times \hat{\mathbf{x}}. \quad (46)$$

It should be pointed out here that the vector integral equations in the previous section are valid in three dimensions as well as in the two-dimensional problem now considered. The only differences are that the field quantities are no longer functions of the longitudinal variable x and that the appropriate two-dimensional Green's function must be used instead of the three-dimensional Green's function. This will be defined when the scalar equations are solved in a later section. For notational purposes, the two-dimensional position vector $\vec{\rho} = y\hat{\mathbf{y}} + z\hat{\mathbf{z}}$ will now be used in regard to the field quantities. Doing so, the tangential field components appearing in equations (40)-(42) can be defined as follows.

$$\hat{\mathbf{z}} \times \vec{\mathbf{H}}(\vec{\rho}) = u(\vec{\rho}) \hat{\mathbf{y}} \quad \text{for } \vec{\rho} \in \sigma \quad (47)$$

$$\hat{\mathbf{n}} \times \vec{\mathbf{H}}(\vec{\rho}) = u(\vec{\rho}) \hat{\mathbf{n}} \times \hat{\mathbf{x}} \quad \text{for } \vec{\rho} \in S \quad (48)$$

$$\hat{\mathbf{z}} \times \vec{\mathbf{E}}(\vec{\rho}) = -\frac{1}{j\omega\epsilon_1} \frac{\partial u(\vec{\rho})}{\partial z} \hat{\mathbf{x}} \quad \text{for } \vec{\rho} \in \sigma \quad (49)$$

$$\hat{\mathbf{z}} \times \vec{\mathbf{H}}^{\text{inc}}(\vec{\rho}) = e^{jk_0(y \cos \theta + z \sin \theta)} \hat{\mathbf{y}} \quad \text{for } \vec{\rho} \in \sigma \quad (50)$$

Now these quantities can be substituted into the vector integral equations, which can then be simplified to produce scalar integral equations.

3.3.1 Scalar Equation 1. The only other term appearing in equation (40) that still needs to be defined is the curl of the dyadic function $\bar{\bar{\Gamma}}$. Recall that it was of the form

$$\bar{\bar{\Gamma}} = -jk\nabla G \times \bar{\bar{\mathbf{I}}} \quad (51)$$

For readability, the arguments of the Green's functions and of the dyadic functions will be suppressed for the remainder of this chapter. Also, in order to indicate which wave number appears in the argument of the Green's functions, it will be understood that $G_1 \equiv G(k_1; \vec{\rho}, \vec{\rho}')$ and $G_0 \equiv G(k_0; \vec{\rho}, \vec{\rho}')$. Given this notation, it can be shown that the curl of the dyadic function in equation (40) can be written as

$$\nabla \times \bar{\bar{\Gamma}} = -jk_1 \left(k_1^2 G_1 \bar{\bar{\mathbf{I}}} + \nabla \nabla G_1 \right) \quad (52)$$

where

$$\nabla \nabla G_1 = \frac{\partial^2 G_1}{\partial y^2} \hat{\mathbf{y}} \hat{\mathbf{y}} + \frac{\partial^2 G_1}{\partial z^2} \hat{\mathbf{z}} \hat{\mathbf{z}} + \frac{\partial^2 G_1}{\partial z \partial y} \hat{\mathbf{y}} \hat{\mathbf{z}} + \frac{\partial^2 G_1}{\partial y \partial z} \hat{\mathbf{z}} \hat{\mathbf{y}} \quad (53)$$

is the Hessian of the two-dimensional Green's function. Substituting each of the newly defined components into the first vector integral equation yields

$$\begin{aligned} & \hat{\mathbf{z}} \times \int_{\sigma} u(\vec{\rho}) \hat{\mathbf{y}} \cdot (-jk_1) \left(k_1^2 G_1 \bar{\bar{\mathbf{I}}} + \nabla \nabla G_1 \right) d\sigma \\ & + \hat{\mathbf{z}} \times \int_S (u(\vec{\rho}) \hat{\mathbf{n}} \times \hat{\mathbf{x}}) \cdot (-jk_1) \left(k_1^2 G_1 \bar{\bar{\mathbf{I}}} + \nabla \nabla G_1 \right) dl = \frac{k_1^2 Y_1}{2j\omega\epsilon_1} \frac{\partial u(\vec{\rho})}{\partial z} \hat{\mathbf{x}}. \end{aligned} \quad (54)$$

Denote the components of the newly formed integral equation as $I + II = III$. To begin simplifying the first part, take the dot product with $\hat{\mathbf{y}}$ as follows.

$$I = \hat{\mathbf{z}} \times \int_{\sigma} \left[u(\vec{\rho}) \hat{\mathbf{y}} (-jk_1^3 G_1) - jk_1 u(\vec{\rho}) \left(\frac{\partial^2 G_1}{\partial y^2} \hat{\mathbf{y}} + \frac{\partial^2 G_1}{\partial z \partial y} \hat{\mathbf{z}} \right) \right] d\sigma \quad (55)$$

Now taking the cross product of $\hat{\mathbf{z}}$ with the integrand reduces I to

$$I = \hat{\mathbf{x}} \int_{\sigma} \left[jk_1^3 u(\vec{\rho}) G_1 + jk_1 u(\vec{\rho}) \frac{\partial^2 G_1}{\partial y^2} \right] d\sigma. \quad (56)$$

The second part of the integral equation can be written as

$$II = \hat{\mathbf{z}} \times \int_S -jk_1 u(\vec{\rho}) \hat{\mathbf{n}} \cdot \left[\hat{\mathbf{x}} \times \left(k_1^2 G_1 \bar{\mathbf{I}} + \nabla \nabla G_1 \right) \right] dl \quad (57)$$

where the identity $(\vec{\mathbf{a}} \times \vec{\mathbf{b}}) \cdot \vec{\mathbf{c}} = \vec{\mathbf{a}} \cdot (\vec{\mathbf{b}} \times \vec{\mathbf{c}})$ has been used [9]. Next, performing the cross product within the integrand yields

$$II = \hat{\mathbf{z}} \times \int_S -jk_1 u(\vec{\rho}) \hat{\mathbf{n}} \cdot \left[k_1^2 G_1 (\hat{\mathbf{z}} \hat{\mathbf{y}} - \hat{\mathbf{y}} \hat{\mathbf{z}}) - \frac{\partial^2 G_1}{\partial z^2} \hat{\mathbf{y}} \hat{\mathbf{z}} - \frac{\partial^2 G_1}{\partial y \partial z} \hat{\mathbf{y}} \hat{\mathbf{y}} + \frac{\partial^2 G_1}{\partial y^2} \hat{\mathbf{z}} \hat{\mathbf{y}} + \frac{\partial^2 G_1}{\partial z \partial y} \hat{\mathbf{z}} \hat{\mathbf{z}} \right] dl. \quad (58)$$

Dotting $\hat{\mathbf{n}}$ into the integrand and then taking the cross product of $\hat{\mathbf{z}}$ with the integrand reduces it to

$$II = \hat{\mathbf{x}} \int_S jk_1 u(\vec{\rho}) \left[n_z \left(k_1^2 G_1 + \frac{\partial^2 G_1}{\partial y^2} \right) - n_y \frac{\partial^2 G_1}{\partial y \partial z} \right] dl \quad (59)$$

where n_y and n_z are the appropriate components of the outward pointing unit normal vector along S . Finally, the right hand side of the first vector integral equation can be written as

$$III = \hat{\mathbf{x}} \frac{k_1}{2j} \frac{\partial u(\vec{\rho})}{\partial z}. \quad (60)$$

Dotting $\hat{\mathbf{x}}$ into both sides of the integral equation represented by the newly formed $I + II = III$, dividing both sides by jk_1 , and simplifying reduces equation (40) to

$$\begin{aligned} \int_{\sigma} u(\vec{\rho}) \left(k_1^2 G_1 + \frac{\partial^2 G_1}{\partial y^2} \right) d\sigma + \int_S u(\vec{\rho}) \left[n_z \left(k_1^2 G_1 + \frac{\partial^2 G_1}{\partial y^2} \right) - n_y \frac{\partial^2 G_1}{\partial y \partial z} \right] dl \\ = \frac{-1}{2} \frac{\partial u(\vec{\rho}')}{\partial z}, \quad \vec{\rho}' \in \sigma. \end{aligned} \quad (61)$$

Equation (61) is now a scalar integral equation which is in a form that can be solved approximately by the numerical MoM algorithm.

3.3.2 *Scalar Equation 2.* Substituting the field components into the second vector integral equation results in

$$\begin{aligned}
& -\hat{\mathbf{z}} \times \int_{\sigma} \frac{-1}{j\omega\epsilon_1} \frac{\partial u(\vec{\rho})}{\partial z} \hat{\mathbf{x}} \cdot \left[\left(k_1^2 G_1 \bar{\mathbf{I}} + \nabla \nabla G_1 \right) - \left(k_0^2 G_0 \bar{\mathbf{I}} + \nabla \nabla G_0 \right) \right] d\sigma \\
& + \frac{jk_1 Z_1 + jk_0 Z_0}{2} u(\vec{\rho}') \hat{\mathbf{y}} - Z_1 \hat{\mathbf{z}} \times \int_S (u(\vec{\rho}) \hat{\mathbf{n}} \times \hat{\mathbf{x}}) \cdot \left(-jk_1 \nabla G_1 \times \bar{\mathbf{I}} \right) dl \\
& = jk_0 Z_0 e^{jk_0(y \cos \theta + z \sin \theta)} \hat{\mathbf{y}} \quad \text{for } \vec{\rho}' \in \sigma.
\end{aligned} \tag{62}$$

As before, break equation (62) into four parts so that it is of the form $I + II + III = IV$. Then the first part can be written as

$$I = \hat{\mathbf{z}} \times \int_{\sigma} \frac{1}{j\omega\epsilon_1} \frac{\partial u(\vec{\rho})}{\partial z} \hat{\mathbf{x}} \cdot \left[\bar{\mathbf{I}} (k_1^2 G_1 - k_0^2 G_0) + \nabla \nabla (G_1 - G_0) \right] d\sigma. \tag{63}$$

Taking the dot product within the integrand reduces the equation to

$$I = \hat{\mathbf{z}} \times \int_{\sigma} \frac{1}{j\omega\epsilon_1} \frac{\partial u(\vec{\rho})}{\partial z} (k_1^2 G_1 - k_0^2 G_0) \hat{\mathbf{x}} d\sigma. \tag{64}$$

Notice that $\hat{\mathbf{x}} \cdot [\nabla \nabla (G_1 - G_0)]$ vanished in the previous step. This is due to the fact that the Green's functions G_1 and G_0 have no x components, so consequently, the Hessian of $G_1 - G_0$ has no x component. Finally, taking the cross product of $\hat{\mathbf{z}}$ with $\hat{\mathbf{x}}$ in I reduces it to

$$I = \hat{\mathbf{y}} \frac{1}{j\omega\epsilon_1} \int_{\sigma} \frac{\partial u(\vec{\rho})}{\partial z} (k_1^2 G_1 - k_0^2 G_0) d\sigma. \tag{65}$$

Part II of equation (62) is already in simplified form. The third part can be reduced by first performing the cross multiplication of the gradient of G_1 with the idemfactor to obtain

$$III = jk_1 Z_1 \hat{\mathbf{z}} \times \int_S (u(\vec{\rho}) \hat{\mathbf{n}} \times \hat{\mathbf{x}}) \cdot \left[\frac{\partial G_1}{\partial y} \hat{\mathbf{x}} \hat{\mathbf{z}} - \frac{\partial G_1}{\partial z} \hat{\mathbf{x}} \hat{\mathbf{y}} + \frac{\partial G_1}{\partial z} \hat{\mathbf{y}} \hat{\mathbf{x}} - \frac{\partial G_1}{\partial y} \hat{\mathbf{z}} \hat{\mathbf{x}} \right] dl. \tag{66}$$

Next, taking the dot product of $\hat{\mathbf{x}}$ with the right side of the integrand, followed by cross multiplying the integrand with $\hat{\mathbf{n}}$ simplifies part III to

$$III = jk_1 Z_1 \hat{\mathbf{z}} \times \int_S u(\vec{\rho}) \left(n_y \frac{\partial G_1}{\partial y} + n_z \frac{\partial G_1}{\partial z} \right) \hat{\mathbf{x}} dl. \tag{67}$$

The kernel of equation (67) is easily recognized as the normal derivative of G_1 . So, cross multiplying $\hat{\mathbf{z}}$ with the integral simplifies it to

$$III = \hat{\mathbf{y}} j k_1 Z_1 \int_S u(\vec{\rho}) \frac{\partial G_1}{\partial n} dl. \quad (68)$$

The right hand side of equation (62) is already in simplified form, so the final step is to take the dot product of $\hat{\mathbf{y}}$ with both sides of the equation represented by $I + II + III = IV$. Doing so gives the second simplified scalar integral equation as

$$\begin{aligned} & \frac{1}{j\omega\epsilon_1} \int_{\sigma} \frac{\partial u(\vec{\rho})}{\partial z} (k_1^2 G_1 - k_0^2 G_0) d\sigma + j k_1 Z_1 \int_S u(\vec{\rho}) \frac{\partial G_1}{\partial n} dl \\ & + \frac{j}{2} u(\vec{\rho}') (k_1 Z_1 + k_0 Z_0) = j k_0 Z_0 e^{j k_0 (y \cos \theta + z \sin \theta)}, \quad \vec{\rho}' \in \sigma. \end{aligned} \quad (69)$$

3.3.3 Scalar Equation 3. Substituting the necessary components into equation (42) simplifies it to

$$\begin{aligned} & 2\hat{\mathbf{n}}' \times \int_{\sigma} u(\vec{\rho}) \hat{\mathbf{y}} \cdot \left(-j k_1 \nabla G_1 \times \bar{\bar{\mathbf{I}}} \right) d\sigma + \\ & \hat{\mathbf{n}}' \times \int_S (u(\vec{\rho}) \hat{\mathbf{n}} \times \hat{\mathbf{x}}) \cdot \left[(-j k_1) \left(\nabla G_D \times \bar{\bar{\mathbf{I}}}_t + \nabla G_N \times \hat{\mathbf{z}} \hat{\mathbf{z}} \right) \right] dl = \frac{j k_1}{2} u(\vec{\rho}') \hat{\mathbf{n}}' \times \hat{\mathbf{x}}, \quad \vec{\rho}' \in S \end{aligned} \quad (70)$$

where $\bar{\bar{\mathbf{I}}}_t = \hat{\mathbf{x}} \hat{\mathbf{x}} + \hat{\mathbf{y}} \hat{\mathbf{y}}$, and G_D and G_N are defined as in equations (17) and (18), respectively. In a similar fashion as before, the first part of the equation, denoted as I , can be rewritten as

$$I = 2\hat{\mathbf{n}}' \times \int_{\sigma} u(\vec{\rho}) \hat{\mathbf{y}} \cdot \left[(-j k_1) \left(\frac{\partial G_1}{\partial y} \hat{\mathbf{x}} \hat{\mathbf{z}} - \frac{\partial G_1}{\partial z} \hat{\mathbf{x}} \hat{\mathbf{y}} + \frac{\partial G_1}{\partial z} \hat{\mathbf{y}} \hat{\mathbf{x}} - \frac{\partial G_1}{\partial y} \hat{\mathbf{z}} \hat{\mathbf{x}} \right) \right] d\sigma. \quad (71)$$

Performing the dot multiplication then gives

$$I = -2j k_1 (\hat{\mathbf{n}}' \times \hat{\mathbf{x}}) \int_{\sigma} u(\vec{\rho}) \frac{\partial G_1}{\partial z} d\sigma \quad (72)$$

as the simplified version of I . The second part of the integral equation can be written as

$$II = -j k_1 \hat{\mathbf{n}}' \times \int_S (u(\vec{\rho}) \hat{\mathbf{n}} \times \hat{\mathbf{x}}) \cdot \left[\frac{-\partial G_D}{\partial z} \hat{\mathbf{x}} \hat{\mathbf{y}} + \frac{\partial G_D}{\partial z} \hat{\mathbf{y}} \hat{\mathbf{x}} - \frac{\partial G_D}{\partial y} \hat{\mathbf{z}} \hat{\mathbf{x}} + \frac{\partial G_N}{\partial y} \hat{\mathbf{x}} \hat{\mathbf{z}} \right] dl \quad (73)$$

where the required cross products have been performed. Again, applying the identity $(\vec{a} \times \vec{b}) \cdot \vec{c} = \vec{a} \cdot (\vec{b} \times \vec{c})$, the second part of the integral equation can be reduced to

$$II = -jk_1 \hat{n}' \times \int_S u(\vec{\rho}) \hat{n} \cdot \left[\frac{\partial G_D}{\partial y} \hat{y} \hat{x} + \frac{\partial G_D}{\partial z} \hat{z} \hat{x} \right] dl. \quad (74)$$

Recognizing the kernel of the integrand in equation (74) as the gradient of G_D being dotted with \hat{n} allows the second part to be simplified as

$$II = -jk_1 (\hat{n}' \times \hat{x}) \int_S u(\vec{\rho}) \frac{\partial G_D}{\partial n} dl. \quad (75)$$

Since the third part of the third integral equation is already simplified, the only thing left to do is to dot the vector $(\hat{n}' \times \hat{x})$ into both sides of the equation represented by $I + II = III$ and divide both sides by $-jk_1$. This gives the final simplified form of the third scalar integral equation as

$$2 \int_\sigma u(\vec{\rho}) \frac{\partial G_1}{\partial z} d\sigma + \int_S u(\vec{\rho}) \frac{\partial G_D}{\partial n} dl = \frac{-1}{2} u(\vec{\rho}'), \quad \vec{\rho}' \in S. \quad (76)$$

Equations (61), (69), and (76) represent the scalar form of the three coupled vector integral equations that govern the electromagnetic scattering from an embedded cavity in a PEC ground plane under TE polarization. The integral equations are now in a form which can be approximately solved for the unknown fields using a numerical technique. The numerical MoM algorithm is developed in the following chapter.

IV. Numerical Solution

In this chapter, the general procedure of solving a linear operator equation via the Method of Moments (MoM) is discussed. This is followed by the development of a MoM algorithm designed to find an approximate solution to the three scalar integral equations (61), (69), and (76). In applying the MoM algorithm, certain singular integrals arise and must be handled properly. This chapter demonstrates how such integrals can be treated so that they can be evaluated numerically. Finally, the error of the MoM algorithm is considered and an estimate of the order of convergence of the method is given.

4.1 Method of Moments

The basic premise behind the Method of Moments is to transform a linear operator equation into a system of simultaneous linear equations. The method was first conceived by a Russian scientist named Galerkin in 1915 to solve elastodynamic problems. Since then many scientific disciplines have utilized the idea to find an approximate solution to problems involving linear integral and differential operators. While many scientists contributed to the development of the theory, in 1967 Roger Harrington of Syracuse University presented a unified approach to solving electrodynamic problems, including the electromagnetic scattering problem, in a generalized moment method formulation [8].

The MoM is applied to problems in which the unknown quantity is embedded in an integrand or is the argument of a differential operator and cannot be solved for analytically. The process of a linear operator acting upon the unknown to produce a functional effect can be written mathematically as

$$L[u] = f, \tag{77}$$

where L is the linear operator, u is the unknown function, and f is the effect or the forcing function. The unknown quantity u is first expanded in terms of a chosen basis function set, that is

$$u = \sum_{n=-\infty}^{\infty} I_n \Psi_n, \tag{78}$$

where the I_n are unknown expansion coefficients and the Ψ_n are functions from the chosen basis set. Obviously, an infinite number of terms cannot be used in the computation of an approximate solution to equation (77), so the series is truncated to a finite number of terms plus a final term which represents all of the truncated terms, i.e. the error ϵ . This is shown by the equation

$$u = \sum_{n=1}^N I_n \psi_n + \epsilon. \quad (79)$$

Substituting the above expression for u into equation (77) gives

$$L \left[\sum_{n=1}^N I_n \psi_n + \epsilon \right] = f, \quad (80)$$

which due to the linearity of L can be written as

$$\sum_{n=1}^N I_n (L[\psi_n]) + r_\epsilon = f. \quad (81)$$

In equation (81), r_ϵ is called the residual. For an accurate approximation it is desirable to minimize the residual. This is accomplished by taking an inner product with a family of testing functions, Θ_m , which are forced to be orthogonal to the residual. That is,

$$\langle \Theta_m, r_\epsilon \rangle = 0, \quad (82)$$

where the inner product is defined to be

$$\langle \Theta_m, \Lambda \rangle = \int_l \Theta_m \cdot \Lambda \, dl. \quad (83)$$

To perform the testing procedure, the inner products of both sides of equation (81) are taken with the testing functions which gives

$$\sum_{n=1}^N I_n \langle L[\psi_n], \Theta_m \rangle + \langle \Theta_m, r_\epsilon \rangle = \langle \Theta_m, f \rangle. \quad (84)$$

Applying the orthogonality condition of equation (82) and rearranging terms results in

$$\langle \Theta_m, f \rangle = \sum_{n=1}^N I_n \langle L[\psi_n], \Theta_m \rangle, \quad \text{for } m = 1, 2, \dots, N. \quad (85)$$

For the choice of N basis functions and N testing functions, the equations in (85) represent a system of N linear equations with N unknowns, the expansion coefficients I_n . This can be written in matrix notation as

$$[V]_{N \times 1} = [Z]_{N \times N} [I]_{N \times 1}, \quad (86)$$

where

$$\begin{aligned} [V]_m &= \langle \Theta_m, f \rangle \\ [Z]_{mn} &= \langle L[\psi_n], \Theta_m \rangle \\ [I]_n &= I_n \end{aligned} \quad (87)$$

for

$$\begin{aligned} m &= 1, 2, \dots, N \\ n &= 1, 2, \dots, N. \end{aligned} \quad (88)$$

In equation (87), $[V]_m$ is often called the voltage vector or the excitation vector, $[Z]_{mn}$ is referred to as the impedance matrix or the coupling matrix, and $[I]_n$ is called the current vector or the solution vector [10].

Oftentimes the integrations involved in calculating the elements of the coupling matrix are difficult to perform, so it is desirable to choose a set of testing functions that will simplify the process. One of the most commonly used techniques to obtain approximate solutions to these integrations is called point matching. The point matching procedure simply requires that equation (81) be satisfied exactly at discrete points, called *match-points*, in the region of interest. This is accomplished by using Dirac delta functions as testing functions. In doing so, the inner product in equation (83) boils down to a function evaluation which can be easily performed [12].

4.2 Cavity Discretization

In order to find approximate solutions to the scalar integral equations (61), (69), and (76), the cavity perimeter $\partial D = \sigma \cup S$ is discretized into non-overlapping segments. Let there be a total of N_1 segments along the cavity aperture σ and a total of N_2 segments along the cavity surface S . The segments are defined by the node points (y_k, z_k, l_k) as in Figure 3. For each node, (y_k, z_k) represent the (y, z) coordinates of the point, and l_k is the arc length measured clockwise from (y_1, z_1) to (y_k, z_k) along ∂D . In the example shown in Figure 3, $N_1 = 2$ and $N_2 = 5$.

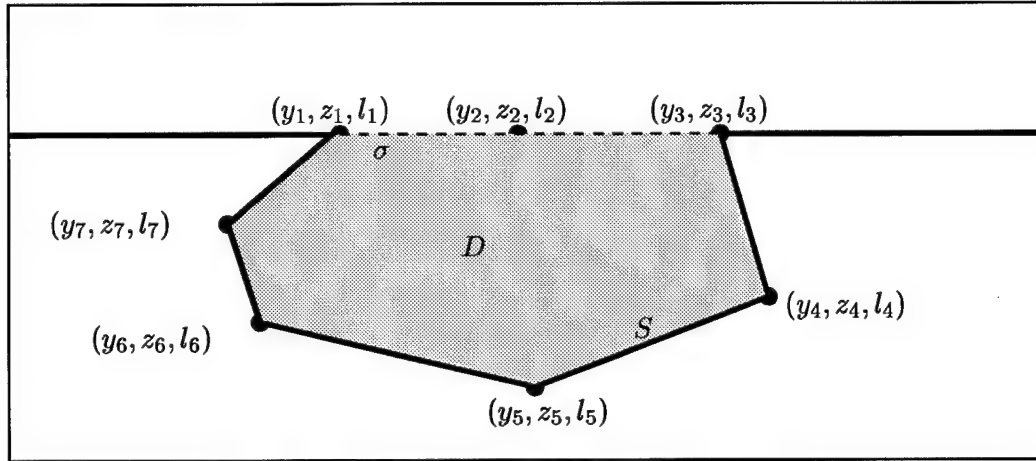


Figure 3 Cavity Discretization

4.3 Method of Moments Algorithm

In this section, the MoM is applied to the three coupled scalar integral equations (61), (69), and (76) to find approximate solutions. The procedure is very similar for all three equations, so some of the details have been omitted from the development of the MoM algorithm for the second and third equations for brevity. Later in the chapter, an explanation of how to program the MoM algorithm on a computer as well as how to deal with certain singular integrals that arise is given.

4.3.1 *Solution Scheme for Equation 1.* In this section the MoM algorithm is developed for the first scalar integral equation. Recall that it is of the form

$$\begin{aligned} \int_{\sigma} u(\vec{\rho}) \left(k_1^2 G_1 + \frac{\partial^2 G_1}{\partial y^2} \right) d\sigma + \int_S u(\vec{\rho}) \left[n_z \left(k_1^2 G_1 + \frac{\partial^2 G_1}{\partial y^2} \right) - n_y \frac{\partial^2 G_1}{\partial y \partial z} \right] dl \\ = \frac{-1}{2} \frac{\partial u(\vec{\rho}')}{\partial z}, \quad \vec{\rho}' \in \sigma \end{aligned} \quad (89)$$

where G_1 is the appropriate two-dimensional Green's function. The unknown quantities in equation (89) are

$$u(\vec{\rho}) \quad \vec{\rho} \in \sigma \quad (90)$$

$$u(\vec{\rho}') \quad \vec{\rho}' \in S \quad (91)$$

$$\frac{\partial u(\vec{\rho})}{\partial z} \quad \vec{\rho} \in \sigma \quad (92)$$

which represent the total magnetic field along the cavity aperture, the total magnetic field along the cavity surface, and the normal derivative of the magnetic field along the cavity aperture, respectively.

The first step in the MoM procedure is to expand the unknowns in terms of the chosen basis function set. Using pulse basis functions, the unknowns in equations (90), (91), and (92) can be approximated as

$$u(l) \approx \sum_{n=1}^{N_1+N_2} a_n p_n(l), \quad \vec{\rho}(l) \in \partial D \quad (93)$$

and

$$\frac{\partial u(l)}{\partial z} \approx \sum_{n=1}^{N_1} b_n p_n(l), \quad \vec{\rho}(l) \in \sigma \quad (94)$$

where a_n and b_n are the unknown expansion coefficients and $p_n(l)$ is the pulse basis function. Note that the vector position functions are now defined in terms of the arc length l along the perimeter of the cavity. The pulse basis function is then defined to be

$$p_n(l) = \begin{cases} 1 & l_n \leq l \leq l_{n+1} \\ 0 & \text{otherwise} \end{cases} \quad (95)$$

As mentioned earlier, Dirac delta functions will be used as the testing functions to employ the point matching technique and simplify calculations. This is defined to be

$$\Theta_m(l) = \delta\left(l - l_{m+\frac{1}{2}}\right) \quad (96)$$

where

$$l_{m+\frac{1}{2}} = \frac{l_m + l_{m+1}}{2} \quad (97)$$

is the midpoint or matchpoint of each segment.

Now the approximations in equations (93) and (94) can be substituted for the unknowns in Equation (89) to produce

$$\begin{aligned} & \sum_{n=1}^{N_1} a_n \int_{l_n}^{l_{n+1}} p_n(l) \left[k_1^2 G_1(l, l') + \frac{\partial^2 G_1(l, l')}{\partial y^2} \right] dl \\ & + \sum_{n=N_1+1}^{N_1+N_2} a_n \int_{l_n}^{l_{n+1}} p_n(l) \left[n_z \left(k_1^2 G_1(l, l') + \frac{\partial^2 G_1(l, l')}{\partial y^2} \right) - n_y \frac{\partial^2 G_1(l, l')}{\partial y \partial z} \right] dl \\ & = \sum_{n=1}^{N_1} \frac{-1}{2} b_n p_n(l). \end{aligned} \quad (98)$$

Next the inner product used will be defined as

$$\langle \Theta_m, \Lambda \rangle = \int_0^\Gamma \Lambda \cdot \delta\left(l' - l_{m+\frac{1}{2}}\right) dl' \quad (99)$$

where Γ is the total arc length around the perimeter of the cavity. Taking the inner product with Θ_m of both sides of equation (98) gives

$$\begin{aligned} & \sum_{n=1}^{N_1} a_n \int_0^\Gamma \int_{l_n}^{l_{n+1}} p_n(l) \left[k_1^2 G_1(l, l') + \frac{\partial^2 G_1(l, l')}{\partial y^2} \right] \delta\left(l' - l_{m+\frac{1}{2}}\right) dl dl' + \\ & \sum_{n=N_1+1}^{N_1+N_2} a_n \int_0^\Gamma \int_{l_n}^{l_{n+1}} p_n(l) \left[n_z \left(k_1^2 G_1(l, l') + \frac{\partial^2 G_1(l, l')}{\partial y^2} \right) - n_y \frac{\partial^2 G_1(l, l')}{\partial y \partial z} \right] \delta\left(l' - l_{m+\frac{1}{2}}\right) dl dl' \\ & = \sum_{n=1}^{N_1} \frac{-1}{2} b_n \int_0^\Gamma p_n(l') \delta\left(l' - l_{m+\frac{1}{2}}\right) dl'. \end{aligned} \quad (100)$$

Using the sifting property of the Dirac delta function, equation (100) simplifies to

$$\begin{aligned}
& \sum_{n=1}^{N_1} a_n \int_{l_n}^{l_{n+1}} \left[k_1^2 G_1 \left(l, l_{m+\frac{1}{2}} \right) + \frac{\partial^2 G_1 \left(l, l_{m+\frac{1}{2}} \right)}{\partial y^2} \right] dl \\
& + \sum_{n=N_1+1}^{N_1+N_2} a_n \int_{l_n}^{l_{n+1}} \left[n_z \left(k_1^2 G_1 \left(l, l_{m+\frac{1}{2}} \right) + \frac{\partial^2 G_1 \left(l, l_{m+\frac{1}{2}} \right)}{\partial y^2} \right) - n_y \frac{\partial^2 G_1 \left(l, l_{m+\frac{1}{2}} \right)}{\partial y \partial z} \right] dl \\
& = \sum_{n=1}^{N_1} \frac{-1}{2} b_n p_n \left(l_{m+\frac{1}{2}} \right).
\end{aligned} \tag{101}$$

This can be written more concisely as

$$\sum_{n=1}^{N_1} a_n \alpha_{mn} + \sum_{n=N_1+1}^{N_1+N_2} a_n \beta_{mn} + \frac{1}{2} \sum_{n=1}^{N_1} b_n = 0 \tag{102}$$

where

$$\alpha_{mn} = \int_{l_n}^{l_{n+1}} \left[k_1^2 G_1 \left(l, l_{m+\frac{1}{2}} \right) + \frac{\partial^2 G_1 \left(l, l_{m+\frac{1}{2}} \right)}{\partial y^2} \right] dl \tag{103}$$

and

$$\beta_{mn} = \int_{l_n}^{l_{n+1}} \left[n_z \left(k_1^2 G_1 \left(l, l_{m+\frac{1}{2}} \right) + \frac{\partial^2 G_1 \left(l, l_{m+\frac{1}{2}} \right)}{\partial y^2} \right) - n_y \frac{\partial^2 G_1 \left(l, l_{m+\frac{1}{2}} \right)}{\partial y \partial z} \right] dl \tag{104}$$

for $m = 1, 2, 3, \dots, N_1$ and $n = 1, 2, 3, \dots, N_1 + N_2$. Equations (103) and (104) can now be used to fill the entries of a matrix of the form

$$A_1 = \begin{bmatrix} \alpha_{1,1} & \cdots & \alpha_{1,N_1} & \beta_{1,N_1+1} & \cdots & \beta_{1,N_1+N_2} & \frac{1}{2} & \cdots & 0 \\ \vdots & \ddots & \vdots & \vdots & \ddots & \vdots & \vdots & \ddots & \vdots \\ \alpha_{N_1,1} & \cdots & \alpha_{N_1,N_1} & \beta_{N_1,N_1+1} & \cdots & \beta_{N_1,N_1+N_2} & 0 & \cdots & \frac{1}{2} \end{bmatrix}. \tag{105}$$

The linear system

$$A_1 \begin{bmatrix} a_n \\ b_n \end{bmatrix} = \begin{bmatrix} 0 \\ \vdots \\ 0 \end{bmatrix} \tag{106}$$

contains $2N_1 + N_2$ unknown expansion coefficients but only N_1 equations. The remaining equations necessary to obtain a unique solution will come from the other two scalar integral equations.

4.3.2 Solution Scheme for Equation 2. In this section the MoM algorithm for the second scalar integral equation is developed. The equation is

$$\begin{aligned} & \frac{1}{j\omega\epsilon_1} \int_{\sigma} \frac{\partial u(\vec{\rho})}{\partial z} (k_1^2 G_1 - k_0^2 G_0) d\sigma + jk_1 Z_1 \int_S u(\vec{\rho}) \frac{\partial G_1}{\partial n} dl \\ & + \frac{j}{2} u(\vec{\rho}') (k_1 Z_1 + k_0 Z_0) = jk_0 Z_0 e^{jk_0(y \cos \theta + z \sin \theta)}, \quad \vec{\rho}' \in \sigma. \end{aligned} \quad (107)$$

Proceeding in a similar fashion as the previous section, pulse basis functions are used to expand the unknowns in terms of the expansion coefficients a_n and b_n . Discretizing equation (107), taking the inner product with the delta testing functions, and rearranging terms gives

$$\begin{aligned} & \frac{1}{j\omega\epsilon_1} \sum_{n=1}^{N_1} b_n \int_{l_n}^{l_{n+1}} \left[k_1^2 G_1 \left(l, l_{m+\frac{1}{2}} \right) - k_0^2 G_0 \left(l, l_{m+\frac{1}{2}} \right) \right] dl \\ & + \frac{j}{2} \sum_{n=1}^{N_1} a_n (k_1 Z_1 + k_0 Z_0) + jk_1 Z_1 \sum_{n=N_1+1}^{N_1+N_2} a_n \int_{l_n}^{l_{n+1}} \frac{\partial G_1 \left(l, l_{m+\frac{1}{2}} \right)}{\partial n} dl \\ & = jk_0 Z_0 e^{jk_0(y_{m+\frac{1}{2}} \cos \theta + z_{m+\frac{1}{2}} \sin \theta)}. \end{aligned} \quad (108)$$

Equation (108) can be written as

$$H \sum_{n=1}^{N_1} a_n + \sum_{n=N_1+1}^{N_1+N_2} a_n \eta_{mn} + \sum_{n=1}^{N_1} b_n \gamma_{mn} = f \left(y_{m+\frac{1}{2}}, z_{m+\frac{1}{2}} \right), \quad (109)$$

where

$$H = \frac{j}{2} (k_1 Z_1 + k_0 Z_0), \quad (110)$$

$$\eta_{mn} = jk_1 Z_1 \int_{l_n}^{l_{n+1}} \frac{\partial G_1 \left(l, l_{m+\frac{1}{2}} \right)}{\partial n} dl, \quad (111)$$

$$\gamma_{mn} = \frac{1}{j\omega\epsilon_1} \int_{l_n}^{l_{n+1}} \left[k_1^2 G_1 \left(l, l_{m+\frac{1}{2}} \right) - k_0^2 G_0 \left(l, l_{m+\frac{1}{2}} \right) \right] dl, \quad (112)$$

and

$$f\left(y_{m+\frac{1}{2}}, z_{m+\frac{1}{2}}\right) = jk_0 Z_0 e^{jk_0(y_{m+\frac{1}{2}} \cos \theta + z_{m+\frac{1}{2}} \sin \theta)} \quad (113)$$

for $m = 1, 2, 3, \dots, N_1$ and $n = 1, 2, 3, \dots, N_1 + N_2$. Now equations (110), (111), and (112) are used to compute the elements of a matrix of the form

$$A_2 = \begin{bmatrix} H & \cdots & 0 & \eta_{1,N_1+1} & \cdots & \eta_{1,N_1+N_2} & \gamma_{1,1} & \cdots & \gamma_{1,N_1} \\ \vdots & \ddots & \vdots & \vdots & \ddots & \vdots & \vdots & \ddots & \vdots \\ 0 & \cdots & H & \eta_{N_1,N_1+1} & \cdots & \eta_{N_1,N_1+N_2} & \gamma_{N_1,1} & \cdots & \gamma_{N_1,N_1} \end{bmatrix}. \quad (114)$$

The system represented by A_2 provides an additional N_1 equations with the same unknowns as the system in (106). The third integral equation will provide the other necessary N_2 equations.

4.3.3 Solution Scheme for Equation 3. In this section the MoM algorithm is developed for the final scalar integral equation which is given by the formula

$$2 \int_{\sigma} u(\vec{\rho}) \frac{\partial G_1}{\partial z} d\sigma + \int_S u(\vec{\rho}) \frac{\partial G_D}{\partial n} dl = \frac{-1}{2} u(\vec{\rho}'), \quad \vec{\rho}' \in S. \quad (115)$$

Following the same procedure as before, equation (115) is discretized using pulse basis functions, and the inner product is taken with the delta testing functions. This results in the equation

$$\begin{aligned} 2 \sum_{n=1}^{N_1} a_n \int_{l_n}^{l_{n+1}} \frac{\partial G_1(l, l_{m+\frac{1}{2}})}{\partial z} dl + \sum_{n=N_1+1}^{N_1+N_2} a_n \int_{l_n}^{l_{n+1}} \frac{\partial G_D(l, l_{m+\frac{1}{2}})}{\partial n} dl \\ = \frac{-1}{2} \sum_{n=N_1+1}^{N_1+N_2} a_n. \end{aligned} \quad (116)$$

This can be more simply written as

$$\sum_{n=1}^{N_1} a_n \psi_{mn} + \sum_{n=N_1+1}^{N_1+N_2} a_n \xi_{mn} + \frac{1}{2} \sum_{n=N_1+1}^{N_1+N_2} a_n = 0, \quad (117)$$

where

$$\psi_{mn} = 2 \int_{l_n}^{l_{n+1}} \frac{\partial G_1(l, l_{m+\frac{1}{2}})}{\partial z} dl \quad (118)$$

and

$$\xi_{mn} = \int_{l_n}^{l_{n+1}} \frac{\partial G_D(l, l_{m+\frac{1}{2}})}{\partial n} dl \quad (119)$$

for $m = N_1 + 1, N_1 + 2, \dots, N_1 + N_2$ and $n = 1, 2, 3, \dots, N_1 + N_2$. Using these equations, the following matrix can be computed

$$A_3 = \begin{bmatrix} \psi_{N_1+1,1} & \cdots & \psi_{N_1+1,N_1} & \xi_{N_1+1,N_1+1} + \frac{1}{2} & \cdots & \xi_{N_1+1,N_1+N_2} & 0 & \cdots & 0 \\ \vdots & \ddots & \vdots & \vdots & \ddots & \vdots & \vdots & \ddots & \vdots \\ \psi_{N_1+N_2,1} & \cdots & \psi_{N_1+N_2,N_1} & \xi_{N_1+N_2,N_1+1} & \cdots & \xi_{N_1+N_2,N_1+N_2} + \frac{1}{2} & 0 & \cdots & 0 \end{bmatrix}. \quad (120)$$

Notice that there is an N_2 by N_1 submatrix of zeros appearing on the right side of A_3 . This is because the unknown in (92) does not appear in equation (115). Using this MoM algorithm, the coupled set of integral equations has been converted to the linear system $Au = f$, where

$$A = \begin{bmatrix} A_1 & A_2 & A_3 \end{bmatrix}^T, \quad (121)$$

$$u = \begin{bmatrix} a_1 & \cdots & a_{N_1+N_2} & b_1 & \cdots & b_{N_1} \end{bmatrix}^T, \quad (122)$$

and

$$f = \begin{bmatrix} 0 & \cdots & 0 & f(l_{1+\frac{1}{2}}) & \cdots & f(l_{N_1+\frac{1}{2}}) & 0 & \cdots & 0 \end{bmatrix}^T. \quad (123)$$

4.4 Computing the Impedance Matrix

Now that the MoM algorithm has been developed, it is necessary to simplify the equations used to compute the elements of the impedance matrix A . For example, equations (103) and (104) are not currently in a form that can be easily implemented in a computer code to produce the elements of A_1 . By applying some common identities and defining some of the expressions in the MoM algorithm, the elements of A can be easily calculated.

Recall the three-dimensional scalar Green's function was defined earlier as

$$G^{3D}(k; \vec{r}, \vec{r}') = \frac{e^{-jkR}}{4\pi R} \quad (124)$$

$$R = |\vec{r} - \vec{r}'|$$

where $\vec{r} = x\hat{x} + y\hat{y} + z\hat{z}$ and $\vec{r}' = x'\hat{x} + y'\hat{y} + z'\hat{z}$ are position vectors in unprimed and primed coordinates, respectively. The two-dimensional Green's function can be found by making use of the identity

$$\int_{-\infty}^{\infty} \frac{e^{-jkR}}{4\pi R} dx = \frac{1}{4j} H_0^{(2)}(k|\vec{\rho} - \vec{\rho}'|) \equiv G^{2D}(k; \vec{\rho}, \vec{\rho}'), \quad (125)$$

where $H_0^{(2)}$ is the Hankel function of the second kind, and again, $\vec{\rho} = \vec{r} \cdot (\hat{y}\hat{y} + \hat{z}\hat{z})$ is the projection of the position vector onto the yz -plane.

For each segment on ∂D defined by $[l_n, l_{n+1}]$, (y_n, z_n) represents the first node point and (y_{n+1}, z_{n+1}) represents the second node point. Using these node points, the components of the position vector along ∂D can be defined in terms of the arc length as

$$y(l) = y_n + \frac{l - l_n}{l_{n+1} - l_n} (y_{n+1} - y_n) \quad (126)$$

and

$$z(l) = z_n + \frac{l - l_n}{l_{n+1} - l_n} (z_{n+1} - z_n). \quad (127)$$

The components of the discrete set of matchpoints, which are the midpoints of the segments, can be expressed as

$$y_{m+\frac{1}{2}} = \frac{y_m + y_{m+1}}{2} \quad (128)$$

$$z_{m+\frac{1}{2}} = \frac{z_m + z_{m+1}}{2}.$$

Using these definitions, the difference $|\vec{\rho} - \vec{\rho}'|$ in equation (125) can be expressed as

$$d_m(l) = \sqrt{\left[y(l) - y_{m+\frac{1}{2}}\right]^2 + \left[z(l) - z_{m+\frac{1}{2}}\right]^2}. \quad (129)$$

Then the two-dimensional Green's function for the MoM algorithm can be expressed as

$$G(k; l, l_{m+\frac{1}{2}}) = \frac{1}{4j} [J_0(k \cdot d_m(l)) - jY_0(k \cdot d_m(l))]. \quad (130)$$

4.4.1 *Computing A_1 .* Recall the α_{mn} elements of A_1 are given by the equation

$$\alpha_{mn} = \int_{l_n}^{l_{n+1}} \left[k_1^2 G_1(l, l_{m+\frac{1}{2}}) + \frac{\partial^2 G_1(l, l_{m+\frac{1}{2}})}{\partial y^2} \right] dl. \quad (131)$$

This can be rewritten as

$$\alpha_{mn} = \int_{l_n}^{l_{n+1}} \left[\frac{k_1^2}{4j} H_0^{(2)}(k_1 d_m(l)) + \frac{1}{4j} \frac{\partial^2 H_0^{(2)}(k_1 d_m(l))}{\partial y^2} \right] dl. \quad (132)$$

Using the properties of Bessel functions, the second derivative term in equation (132) can be simplified to

$$\frac{\partial^2 H_0^{(2)}(k_1 d_m(l))}{\partial y^2} = k_1^2 \left[-H_0^{(2)}(k_1 d_m(l)) + \frac{1}{k_1 d_m(l)} H_1^{(2)}(k_1 d_m(l)) \right]. \quad (133)$$

Plugging this expression back into equation (132) for the second derivative term and simplifying reduces to

$$\alpha_{mn} = \int_{l_n}^{l_{n+1}} \frac{k_1}{4j d_m(l)} H_1^{(2)}(k_1 d_m(l)) dl. \quad (134)$$

where $H_1^{(2)}(k_1 d_m(l)) = J_1(k_1 d_m(l)) - jY_1(k_1 d_m(l))$ is the first order Hankel function of the second kind.

Equation (134) can now be easily implemented in a computer code. However, care must be taken when $m = n$, that is when the integration is performed over a segment containing the current match point. When $m = n$, $d_m(l) = 0$ at each matchpoint $(y_{m+\frac{1}{2}}, z_{m+\frac{1}{2}})$ and the expression in equation (134) becomes a singular integral. There are many techniques for handling the numerical integration of such singular integrals. One of the most efficient techniques is to remove the singularity from the integrand, integrate the singularity analytically if possible, then add its contribution back to the original integral. In order to apply this technique to the current problem, the singular nature of the

integrand must first be understood. In the limit as the argument of the Neumann function goes to zero [6],

$$Y_1(x) \approx \frac{-2}{\pi x} \quad \text{as } x \rightarrow 0^+. \quad (135)$$

Given this asymptotic approximation, consider removing the singularity from the integrand of equation (134) in the following manner.

$$\begin{aligned} \alpha_{mn} = & \int_{l_n}^{l_{n+1}} \frac{k_1}{4jd_m(l)} \left[J_1(k_1 d_m(l)) - jY_1(k_1 d_m(l)) - \frac{2j}{\pi k_1 d_m(l)} \right] dl \\ & + \lim_{\delta \rightarrow 0^+} \int_{l_n}^{l_{n+1}} \frac{1}{2\pi [d_m(l) + \delta]^2} dl. \end{aligned} \quad (136)$$

Now the first integral in equation (136) can be integrated numerically, and the second integral can be computed analytically to determine its contribution to the entire integral. This is done by performing the integration and then taking the limit as δ goes to 0 as shown below.

$$\begin{aligned} \lim_{\delta \rightarrow 0^+} \int_{l_n}^{l_{n+1}} \frac{1}{2\pi [d_m(l) + \delta]^2} dl &= \frac{1}{2\pi} \left[\frac{1}{y_{m+\frac{1}{2}} - l_{n+1}} - \frac{1}{y_{m+\frac{1}{2}} - l_n} \right] \\ &= \frac{1}{2\pi} \left[\frac{-2}{l_{n+1} - l_n} - \frac{2}{l_{n+1} - l_n} \right] = \frac{-2}{\pi (l_{n+1} - l_n)}. \end{aligned} \quad (137)$$

So in order to numerically calculate the diagonal entries of the α_{mn} submatrix (where $m = n$), the following formula can be used

$$\alpha_{mn} = \int_{l_n}^{l_{n+1}} \frac{k_1}{4jd_m(l)} \left[J_1(k_1 d_m(l)) - jY_1(k_1 d_m(l)) - \frac{2j}{\pi k_1 d_m(l)} \right] dl - \frac{2}{\pi (l_{n+1} - l_n)}. \quad (138)$$

The β_{mn} elements of A_1 are found using the formula

$$\beta_{mn} = \int_{l_n}^{l_{n+1}} \left[n_z \left(k_1^2 G_1 \left(l, l_{m+\frac{1}{2}} \right) + \frac{\partial^2 G_1 \left(l, l_{m+\frac{1}{2}} \right)}{\partial y^2} \right) - n_y \frac{\partial^2 G_1 \left(l, l_{m+\frac{1}{2}} \right)}{\partial y \partial z} \right] dl. \quad (139)$$

Notice that in order to calculate these integrals it will be necessary to find an expression for the components of the outward pointing normal vector along ∂D as well as another partial derivative of the two-dimensional Green's function. First, to obtain the normal

vector, define a unit vector that is tangent to the perimeter of the cavity pointing in the clockwise direction. That is,

$$\hat{\mathbf{l}}_n = \frac{(y_{n+1} - y_n) \hat{\mathbf{y}} + (z_{n+1} - z_n) \hat{\mathbf{z}}}{l_{n+1} - l_n}. \quad (140)$$

Then the unit normal vector pointing out from the surface and aperture of the cavity can be found by taking the cross product of $\hat{\mathbf{x}}$ with $\hat{\mathbf{l}}_n$. This results in

$$\hat{\mathbf{n}} = \hat{\mathbf{x}} \times \hat{\mathbf{l}}_n = -\hat{\mathbf{y}} \frac{z_{n+1} - z_n}{l_{n+1} - l_n} + \hat{\mathbf{z}} \frac{y_{n+1} - y_n}{l_{n+1} - l_n}. \quad (141)$$

This gives the components of the unit normal vector required in equation (139). Specifically, they are

$$\begin{aligned} n_y &= -\frac{z_{n+1} - z_n}{l_{n+1} - l_n} \\ n_z &= \frac{y_{n+1} - y_n}{l_{n+1} - l_n} \end{aligned} \quad (142)$$

Given that

$$G_1 \left(l, l_{m+\frac{1}{2}} \right) = \frac{1}{4j} H_0^{(2)} (k_1 d_m(l)), \quad (143)$$

it was found in the previous section that

$$\frac{\partial^2 H_0^{(2)} (k_1 d_m(l))}{\partial y^2} = k_1^2 \left[-H_0^{(2)} (k_1 d_m(l)) + \frac{1}{k_1 d_m(l)} H_1^{(2)} (k_1 d_m(l)) \right]. \quad (144)$$

Furthermore, it can be shown that

$$\begin{aligned} \frac{\partial^2 H_0^{(2)} (k_1 d_m(l))}{\partial y \partial z} = \\ k_1^2 \frac{(y(l) - y_{m+\frac{1}{2}}) (z(l) - z_{m+\frac{1}{2}})}{[d_m(l)]^2} \left[-H_0^{(2)} (k_1 d_m(l)) + \frac{2H_1^{(2)} (k_1 d_m(l))}{k_1 d_m(l)} \right]. \end{aligned} \quad (145)$$

Substituting these expressions back into equation (139) and simplifying the results gives a more useful form of the β_{mn} equation. That is,

$$\begin{aligned} \beta_{mn} = & \int_{l_n}^{l_{n+1}} \frac{k_1^2}{4j} H_0^{(2)}(k_1 d_m(l)) \left[n_z + \frac{(y(l) - y_{m+\frac{1}{2}})^2}{[d_m(l)]^2} \left(-n_z + n_y \frac{(z(l) - z_{m+\frac{1}{2}})}{(y(l) - y_{m+\frac{1}{2}})} \right) \right] \\ & + \frac{k_1}{4j} H_1^{(2)}(k_1 d_m(l)) \left[n_z \frac{(y(l) - y_{m+\frac{1}{2}})^2}{[d_m(l)]^3} \left(2 - \frac{[d_m(l)]^2}{(y(l) - y_{m+\frac{1}{2}})^2} \right) \right] \\ & + \frac{k_1}{4j} H_1^{(2)}(k_1 d_m(l)) \frac{2n_y}{[d_m(l)]^3} (y(l) - y_{m+\frac{1}{2}}) (z(l) - z_{m+\frac{1}{2}}) dl. \end{aligned} \quad (146)$$

Equation (146) can now be easily implemented in a computer code to calculate the β_{mn} elements of the impedance matrix. Also, since $m = 1, 2, \dots, N_1$ and $n = N_1 + 1, N_1 + 2, \dots, N_1 + N_2$, $\vec{\rho}(l) \in S$ and $\vec{\rho}'(l) \in \sigma$. In other words, the match points for the β_{mn} entries all lie on the cavity aperture σ and the integrations are all performed over segments on the cavity surface S . So the metric $d_m(l)$ is never 0 and the integrand in equation (146) is never singular.

4.4.2 Computing A_2 . The first N_1 by N_1 submatrix of the A_2 matrix is composed of all zeros except for the diagonal elements. They are all constant and are given by the expression

$$H = \frac{j}{2} (k_1 Z_1 + k_0 Z_0), \quad (147)$$

which can be easily calculated in the computer code.

Recall that the η_{mn} terms are given by the formula

$$\eta_{mn} = j k_1 Z_1 \int_{l_n}^{l_{n+1}} \frac{\partial G_1(l, l_{m+\frac{1}{2}})}{\partial n} dl. \quad (148)$$

Rewriting this equation with the equivalent form of the two-dimensional Green's function gives

$$\eta_{mn} = \frac{k_1 Z_1}{4} \int_{l_n}^{l_{n+1}} \frac{\partial H_0^{(2)}(k_1 d_m(l))}{\partial n} dl, \quad (149)$$

which requires the computation of the normal derivative of the Hankel function. The normal derivative of a continuous function f with continuous first and second partial derivatives in a region defined by a simply connected path C is given by the formula

$$\frac{\partial f}{\partial n} = \hat{\mathbf{n}} \cdot \nabla f, \quad (150)$$

where $\hat{\mathbf{n}}$ is the outward pointing unit normal vector to C [20]. In order to compute the normal derivative in equation (149), define the unit normal vector in the same manner as the previous section. That is,

$$\hat{\mathbf{n}} = -\hat{\mathbf{y}} \frac{z_{n+1} - z_n}{l_{n+1} - l_n} + \hat{\mathbf{z}} \frac{y_{n+1} - y_n}{l_{n+1} - l_n}. \quad (151)$$

The gradient of the Hankel function can be shown to be

$$\begin{aligned} \nabla H_0^{(2)}(k_1 d_m(l)) &= -k_1 \frac{(y(l) - y_{m+\frac{1}{2}})}{d_m(l)} H_1^{(2)}(k_1 d_m(l)) \hat{\mathbf{y}} \\ &\quad - k_1 \frac{(z(l) - z_{m+\frac{1}{2}})}{d_m(l)} H_1^{(2)}(k_1 d_m(l)) \hat{\mathbf{z}}. \end{aligned} \quad (152)$$

Taking the dot product of $\hat{\mathbf{n}}$ with equation (152), plugging back into equation (149) and simplifying results in

$$\eta_{mn} = \int_{l_n}^{l_{n+1}} Z_1 \frac{k_1^2}{4d_m(l)} H_1^{(2)}(k_1 d_m(l)) \left[-n_y (y(l) - y_{m+\frac{1}{2}}) - n_z (z(l) - z_{m+\frac{1}{2}}) \right] dl, \quad (153)$$

which is now in a form that can be computed numerically. Notice that in this case, $\vec{\rho}(l) \in S$ and $\vec{\rho}'(l) \in \sigma$ since all of the matchpoints are contained in segments along the aperture while the integrations are performed over segments along the surface S . So the expression $d_m(l)$ will never be zero and there are no singularities to consider.

The γ_{mn} elements of the A_2 matrix are given by the formula

$$\gamma_{mn} = \frac{1}{j\omega\epsilon_1} \int_{l_n}^{l_{n+1}} \left[k_1^2 G_1(l, l_{m+\frac{1}{2}}) - k_0^2 G_0(l, l_{m+\frac{1}{2}}) \right] dl, \quad (154)$$

which when rewritten with the appropriate Hankel functions substituted in for the two-dimensional Green's functions appears as

$$\gamma_{mn} = \frac{1}{j\omega\epsilon_1} \int_{l_n}^{l_{n+1}} \left[\frac{k_1^2}{4j} H_0^{(2)}(k_1 d_m(l)) - \frac{k_0^2}{4j} H_0^{(2)}(k_0 d_m(l)) \right] dl. \quad (155)$$

In the case where $m \neq n$, equation (155) can be readily implemented in a computer code to produce the γ_{mn} elements of A_2 . However, since $\bar{\rho}(l) \in \sigma$ and $\bar{\rho}'(l) \in \sigma$, $d_m(l)$ will be zero at the matchpoints. This will make the Neumann functions in the integrand of equation (155) singular when $m = n$. In order to efficiently calculate the numerical integration in these instances, again consider removing the singularity, integrating it analytically, and adding its contribution back to the total integral. Notice, however, that in the degenerate case ($k_0 = k_1$, i.e. an unfilled cavity) the integrand in equation (155) will be zero for every value of m and n . In this case, the γ_{mn} submatrix may simply be set to all zeros with no treatment of the singularity necessary.

The asymptotic small argument approximation of the zeroth order Neumann function is given by

$$Y_0(x) \approx \frac{2}{\pi} \ln\left(\frac{\gamma x}{2}\right) \quad \text{as } x \rightarrow 0^+, \quad (156)$$

where $\gamma \approx 1.7810724$ is Euler's coefficient [20]. Since the two Hankel functions appearing in equation (155) differ by only the wave number k_i in their argument, a general treatment of how to remove the singularity where the wave number is simply k will be given for brevity. Consider the equation

$$\tilde{\gamma}_{mn} = \int_{l_n}^{l_{n+1}} H_0^{(2)}(k d_m(l)) dl. \quad (157)$$

The singularity in the Neumann function can be removed by writing

$$\begin{aligned} \tilde{\gamma}_{mn} = \int_{l_n}^{l_{n+1}} J_0(k d_m(l)) - j \left[Y_0(k d_m(l)) - \frac{2}{\pi} \ln \frac{\gamma k d_m(l)}{2} \right] dl \\ - \int_{l_n}^{l_{n+1}} \frac{2j}{\pi} \ln \frac{\gamma k d_m(l)}{2} dl. \end{aligned} \quad (158)$$

The first integral in equation (158) can now be numerically calculated in the computer code without any problems, while the second integral contains the removed singularity. In order to integrate the singularity analytically, consider splitting up the natural logarithm in the following manner.

$$I_{\text{sing}} = -\frac{2j}{\pi} \int_{l_n}^{l_{n+1}} \ln \frac{\gamma k}{2} + \ln(d_m(l)) dl. \quad (159)$$

By breaking the integral up, the first term in the integrand is simply a constant and the second term can be integrated by carefully considering its nature. Begin by integrating the constant piece.

$$I_{\text{sing}} = -\frac{2j}{\pi} \ln \left(\frac{\gamma k}{2} \right) (l_{n+1} - l_n) - \frac{2j}{\pi} \int_{l_n}^{l_{n+1}} \ln(d_m(l)) dl. \quad (160)$$

The natural logarithm term in the remaining integral is symmetric about the matchpoint, so the integral can be rewritten as

$$I_{\text{sing}} = -\frac{2j}{\pi} \ln \left(\frac{\gamma k}{2} \right) (l_{n+1} - l_n) - \frac{4j}{\pi} \int_{l_{n+\frac{1}{2}}}^{l_{n+1}} \ln(l - l_{n+\frac{1}{2}}) dl, \quad (161)$$

or equivalently as

$$I_{\text{sing}} = -\frac{2j}{\pi} \ln \left(\frac{\gamma k}{2} \right) (l_{n+1} - l_n) - \frac{4j}{\pi} \int_0^{(l_{n+1}-l_n)/2} \ln(l) dl. \quad (162)$$

Integrating the natural logarithm and simplifying gives the contribution of the removed singularity as

$$I_{\text{sing}} = \frac{2j(l_{n+1} - l_n)}{\pi} \left[1 - \ln \left(\frac{\gamma k(l_{n+1} - l_n)}{4} \right) \right]. \quad (163)$$

If $l_{n+1} - l_n$ is denoted as Δ_n , the treated form of equation (155) can be written as

$$\begin{aligned} \gamma_{mn} = & -\frac{k_1^2}{4\omega\epsilon_1} \left\{ \int_{l_n}^{l_{n+1}} H_0^{(2)}(k_1 d_m(l)) + \frac{2j}{\pi} \ln \frac{\gamma k_1 d_m(l)}{2} dl + \frac{2j\Delta_n}{\pi} \left[1 - \ln \left(\frac{\gamma k_1 \Delta_n}{4} \right) \right] \right\} \\ & + \frac{k_0^2}{4\omega\epsilon_1} \left\{ \int_{l_n}^{l_{n+1}} H_0^{(2)}(k_0 d_m(l)) + \frac{2j}{\pi} \ln \frac{\gamma k_0 d_m(l)}{2} dl + \frac{2j\Delta_n}{\pi} \left[1 - \ln \left(\frac{\gamma k_0 \Delta_n}{4} \right) \right] \right\}. \end{aligned} \quad (164)$$

4.4.3 *Computing A_3 .* Finally, the elements of the A_3 matrix must be computed.

The ψ_{mn} elements are given by the equation

$$\psi_{mn} = 2 \int_{l_n}^{l_{n+1}} \frac{\partial G_1(l, l_{m+\frac{1}{2}})}{\partial z} dl. \quad (165)$$

This is rewritten with the appropriate two-dimensional Green's function as

$$\psi_{mn} = \frac{1}{2j} \int_{l_n}^{l_{n+1}} \frac{\partial H_0^{(2)}(k_1 d_m(l))}{\partial z} dl. \quad (166)$$

The partial derivative of the Hankel function with respect to z is

$$\frac{\partial H_0^{(2)}(k_1 d_m(l))}{\partial z} = -\frac{k_1 (z(l) - z_{m+\frac{1}{2}})}{d_m(l)} H_1^{(2)}(k_1 d_m(l)). \quad (167)$$

So equation (165) can be expressed as

$$\psi_{mn} = -\frac{k_1}{2j} \int_{l_n}^{l_{n+1}} \frac{(z(l) - z_{m+\frac{1}{2}})}{d_m(l)} H_1^{(2)}(k_1 d_m(l)) dl, \quad (168)$$

which is now in a form that can be readily implemented in a computer code. Notice also that since $\vec{\rho}(l) \in \sigma$ and $\vec{\rho}'(l) \in S$ there is no singularity to consider when performing the numerical integration.

The ξ_{mn} elements of the A_3 matrix were found to be given by the equation

$$\xi_{mn} = \int_{l_n}^{l_{n+1}} \frac{\partial G_D(l, l_{m+\frac{1}{2}})}{\partial n} dl. \quad (169)$$

In this equation, G_D is defined to be

$$G_D(k_1; \vec{\rho}, \vec{\rho}') = G(k_1; \vec{\rho}, \vec{\rho}') - G(k_1; \vec{\rho}, \vec{\rho}'_i) \quad (170)$$

where

$$\vec{\rho}'_i = y' \hat{y} - z' \hat{z} \quad (171)$$

is the reflection of the position vector $\vec{\rho}'(l)$ across the aperture of the cavity. For calculations involving $G(k_1; \vec{\rho}, \vec{\rho}'_i)$, a new metric for $|\vec{\rho}(l) - \vec{\rho}'(l)|$ must be employed. Define

$$d_m^i(l) = \sqrt{\left[y(l) - y_{m+\frac{1}{2}}\right]^2 + \left[z(l) + z_{m+\frac{1}{2}}\right]^2} \quad (172)$$

to be such a metric. Then taking the gradient of $G(k_1; \vec{\rho}, \vec{\rho}')$ and of $G(k_1; \vec{\rho}, \vec{\rho}'_i)$ as before, and using the same unit normal vector as defined in equation (151), the normal derivative of $G_D(k_1; \vec{\rho}, \vec{\rho}'_i)$ can be found. Doing so allows equation (169) to be rewritten as

$$\begin{aligned} \xi_{mn} = & \frac{jk_1}{4} \int_{l_n}^{l_{n+1}} \left[n_y \frac{\left(y(l) - y_{m+\frac{1}{2}}\right)}{d_m(l)} + n_z \frac{\left(z(l) - z_{m+\frac{1}{2}}\right)}{d_m(l)} \right] H_1^{(2)}(k_1 d_m(l)) \\ & - \left[n_y \frac{\left(y(l) - y_{m+\frac{1}{2}}\right)}{d_m^i(l)} + n_z \frac{\left(z(l) + z_{m+\frac{1}{2}}\right)}{d_m^i(l)} \right] H_1^{(2)}(k_1 d_m^i(l)) dl. \end{aligned} \quad (173)$$

Even though $\vec{\rho}(l) \in S$ and $\vec{\rho}'(l) \in S$, notice that the newly defined metric in equation (172) will never be zero. So there will be no trouble with singularities when numerically integrating the Hankel function that involves $d_m^i(l)$. However, the Hankel function that contains $d_m(l)$ may pose some problems when the numerical integration is performed over a segment containing the current matchpoint. So if $m = n$, the singularity should be extracted and integrated separately. The same procedure presented in equations (135)-(138) can be followed to remove the singularity by subtracting out the asymptotic small argument approximation of the first order Neumann function from the integrand and integrating it separately.

It should be pointed out here that the singularities that arise in filling the diagonal elements of the α_{mn} and ξ_{mn} submatrices are quite strong. There is another much more easily implemented method of dealing with such strong singularities that is commonly used in computational electromagnetics. Essentially this involves redefining the coordinates of the matchpoint when calculating the self-impedance terms (where $m = n$). By "bumping" the matchpoint a distance of say one hundredth of a wavelength away from the cavity along the outward pointing normal vector, the metric $d_m(l)$ will never actually be zero.

This will allow the numerical integration to be performed, and any error introduced in the solution when the system is solved should be negligible.

Another similar method of dealing with strong singular integrals in computational electromagnetics is the method of equivalent separation. Using this method, a small incremental distance is added to $d_m(l)$ on every segment [10]. This is another way of not allowing the argument of the Hankel functions to ever be zero, thereby obtaining finite values when the integrations are performed. However, this technique introduces a phase error into the integrands, which can have a significant effect on the accuracy of the solution.

4.5 Error Estimate

In this section an estimate of the order of convergence of the MoM algorithm is developed. Consider using a mesh of equally sized segments to discretize the perimeter of the cavity ∂D . Let h be the length of each segment. In the L^2 -norm, the total error in the approximation of $u(l)$ is given by

$$\|e_h\|_{L^2} = \sqrt{\sum_{n \in \partial D} \int_{l_n}^{l_{n+1}} |u(l) - u_{h_n}|^2 dl}. \quad (174)$$

where u_{h_n} is the approximate average value (a constant) of $u(l)$ on each segment defined by $[l_n, l_{n+1}]$ [5]. Notice that the approximation u_{h_n} as well as the interval $[l_n, l_{n+1}]$ depend on the mesh size h . Since a point matching scheme was used at the midpoint of each segment, $u(c_n) = u_{h_n}$ for every midpoint $c_n = (l_{n+1} - l_n)/2$. Furthermore, by the Mean-Value theorem, there exists a point d_n in each interval $[l_n, l_{n+1}]$ such that

$$\|e_h\|_{L^2} \leq \sqrt{\sum_{n \in \partial D} \int_{l_n}^{l_{n+1}} |u'(d_n) \cdot (l - c_n)|^2 dl}. \quad (175)$$

Taking the maximum of $|l - c_n|$ on each segment gives

$$\|e_h\|_{L^2} \leq \sqrt{\sum_{n \in \partial D} \int_{l_n}^{l_{n+1}} \left| u'(d_n) \cdot \frac{h}{2} \right|^2 dl}. \quad (176)$$

Now taking the maximum of $u'(l)$ on each segment and doing the integration reduces the inequality in (176) to

$$\|e_h\|_{L^2} \leq \sqrt{\sum_{n \in \partial D} \max u'(l) \cdot \frac{h^3}{4}}. \quad (177)$$

Since equally sized segments were used to discretize the cavity, the summation under the square root can be replaced giving

$$\|e_h\|_{L^2} \leq \sqrt{\frac{\Gamma}{h} \cdot \max u'(l) \cdot \frac{h^3}{4}}, \quad (178)$$

where Γ is the total arc length along the perimeter ∂D . Finally, simplifying gives the error estimate in the L^2 -norm as

$$\|e_h\|_{L^2} \leq \frac{h}{2} \sqrt{\Gamma \cdot \max u'(l)} \equiv C \cdot h = \mathcal{O}(h). \quad (179)$$

According to (179), if a total of N segments are used along ∂D to approximate $u(l)$, and then the mesh is refined by cutting the length of each segment in half for a total of $2N$ segments, the error in the approximation of $u(l)$ should be cut approximately in half. This estimate of the order of convergence will be examined in the next chapter by considering the relative error in the solutions of several test cavities.

V. Numerical Results

In this chapter, the integral equation method is applied to several test cavities to calculate their monostatic RCS signatures. The results found are then compared with those found by RAM2D [7] and by a hybrid finite element/Fourier transform code [25], and the method is shown to be very accurate. The chapter also contains some error history plots which agree with the predicted convergence estimate presented in the previous chapter.

5.1 Computing the Monostatic RCS

Once the unknown fields have been computed for a given incident angle, a method for calculating the backscatter RCS is required. In order to develop such a method, consider the following mathematical definition of the RCS of a two-dimensional target.

$$\sigma_{2-D} = \lim_{|\vec{\rho}'| \rightarrow \infty} 2\pi |\vec{\rho}'| \frac{|\vec{\mathbf{E}}^s(\vec{\rho}')|^2}{|\vec{\mathbf{E}}^{inc}(\vec{\rho}')|^2}, \quad (180)$$

where $|\vec{\rho}'| = \rho'$ is the distance from the target to the observer, and $\vec{\mathbf{E}}^s$ and $\vec{\mathbf{E}}^{inc}$ are the scattered and incident electric fields, respectively [6]. Recall the radiation integral given by Application 5 in equation (33) was

$$\frac{-jk_0}{2} \vec{\mathbf{E}}^s(\vec{\rho}') = \int_{\sigma} \hat{\mathbf{z}} \times \vec{\mathbf{E}}(\vec{\rho}) \cdot \bar{\bar{\Gamma}}(k_0; \vec{\rho}, \vec{\rho}') d\sigma. \quad (181)$$

This will give the necessary numerator in equation (180). The denominator is already known since it is simply the given incident electric field. In order to compute $\vec{\mathbf{E}}^s(\vec{\rho}')$ in terms of the magnetic fields, apply Maxwell's equation (2) to obtain

$$\vec{\mathbf{E}}^s(\vec{\rho}') = \frac{2j}{k_0} \int_{\sigma} \hat{\mathbf{z}} \times \left(\frac{1}{j\omega\epsilon_0} \nabla \times \vec{\mathbf{H}}(\vec{\rho}) \right) \cdot \bar{\bar{\Gamma}}(k_0; \vec{\rho}, \vec{\rho}') d\sigma. \quad (182)$$

Letting $\vec{\mathbf{H}}(\vec{\rho}) \equiv u\hat{\mathbf{x}}$, perform the two vector cross products and substitute the appropriate expression in for $\bar{\bar{\Gamma}}$ to reduce the equation to

$$\vec{\mathbf{E}}^s(\vec{\rho}') = \frac{-2}{k_0\omega\epsilon_0} \int_{\sigma} \frac{\partial u}{\partial z} \hat{\mathbf{x}} \cdot \left(-jk_0 \nabla G_0 \times \bar{\bar{\mathbf{I}}} \right) d\sigma. \quad (183)$$

Cross multiplying the gradient of the Green's function with the idemfactor and dotting the result with $\hat{\mathbf{x}}$ simplifies the scattered electric field to

$$\vec{\mathbf{E}}^s(\vec{\rho}') = \frac{2j}{\omega\epsilon_0} \int_{\sigma} \frac{\partial u}{\partial z} \left(\frac{\partial G_0}{\partial y} \hat{\mathbf{z}} - \frac{\partial G_0}{\partial z} \hat{\mathbf{y}} \right) d\sigma. \quad (184)$$

Denote

$$\tilde{R} = \sqrt{(y - y')^2 + (z - z')^2} \quad (185)$$

so that

$$G_0 = \frac{1}{4j} H_0^{(2)}(k_0 \tilde{R}). \quad (186)$$

Then taking the appropriate partial derivatives of the Hankel function allows equation (184) to be rewritten as

$$\vec{\mathbf{E}}^s(\vec{\rho}') = \frac{k_0}{2\omega\epsilon_0} \int_{\sigma} \frac{\partial u}{\partial z} H_1^{(2)}(k_0 \tilde{R}) \left(\hat{\mathbf{y}} \frac{z - z'}{\tilde{R}} - \hat{\mathbf{z}} \frac{y - y'}{\tilde{R}} \right) d\sigma. \quad (187)$$

Considering the geometry in Figure 4, it is apparent that $\tilde{R} \approx \rho'$ as $|\vec{\rho}'| \rightarrow \infty$ since y and z are restricted to the aperture of the cavity. Furthermore, since $z \in \sigma$, $z = 0$ and \tilde{R} can be rewritten as

$$\tilde{R} = \sqrt{(y - y')^2 + (z')^2}. \quad (188)$$

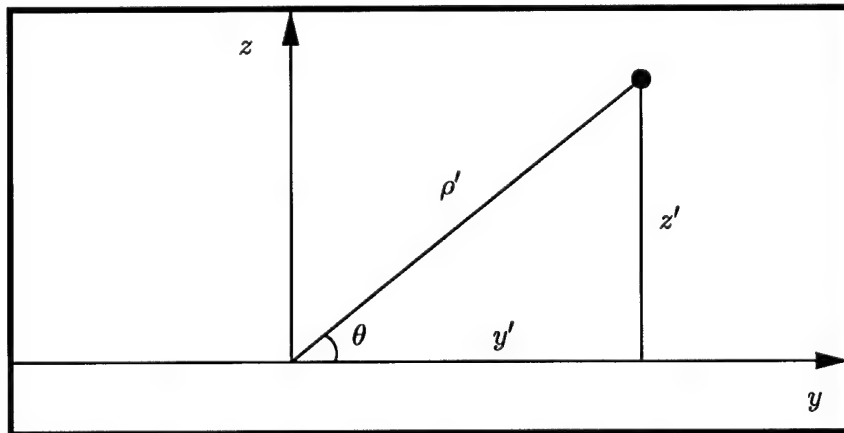


Figure 4 Geometry of $\vec{\rho}'$

This can be further simplified to

$$\begin{aligned}
\tilde{R} &= \sqrt{y^2 - 2y'y + (y')^2 + (z')^2} \\
&= \sqrt{(\rho')^2 + y^2 - 2y'y} \\
&= \sqrt{(\rho')^2 + y^2 - 2y\rho' \cos(\theta)} \\
&= \rho' \sqrt{1 + \left(\frac{y}{\rho'}\right)^2 - \frac{2y \cos(\theta)}{\rho'}} \\
&= \rho' - y \cos(\theta) + \mathcal{O}\left(\frac{1}{\rho'}\right)
\end{aligned} \tag{189}$$

In the limit as $\tilde{R} \rightarrow \infty$, the large argument approximation of the Hankel function is

$$\lim_{\tilde{R} \rightarrow \infty} H_1^{(2)}(k_0 \tilde{R}) \approx \sqrt{\frac{2}{j\pi k_0 \tilde{R}}} e^{-jk_0 \tilde{R}}. \tag{190}$$

This allows the scattered electric field to be approximated as

$$\vec{\mathbf{E}}^s(\vec{\rho}') \approx \frac{1}{\omega \epsilon_0} \sqrt{\frac{k_0}{2j\pi}} \int_{\sigma} \frac{\partial u}{\partial z} e^{-jk_0 \rho'} e^{jk_0 y \cos(\theta)} e^{-jk_0 \mathcal{O}(\frac{1}{\rho'})} \left(-\hat{\mathbf{y}} \frac{z'}{\tilde{R}^{3/2}} - \hat{\mathbf{z}} \frac{y - y'}{\tilde{R}^{3/2}} \right) d\sigma. \tag{191}$$

Recall the incident electric field was given as

$$\vec{\mathbf{E}}^{\text{inc}}(\vec{\rho}') = Z_0 (\sin \theta \hat{\mathbf{y}} - \cos \theta \hat{\mathbf{z}}) e^{jk_0 (y \sin \theta + z \cos \theta)}. \tag{192}$$

Now, plugging equations (191) and (192) into (180) and simplifying yields

$$\sigma_{2\text{-D}} \approx 2\pi \frac{\left| Z_0 \sqrt{\frac{1}{2j\pi k_0}} \int_{\sigma} \frac{\partial u}{\partial z} e^{jk_0 y \cos(\theta)} \lim_{\rho' \rightarrow \infty} \left(-\hat{\mathbf{y}} \frac{\sqrt{\rho'} z'}{\tilde{R}^{3/2}} - \hat{\mathbf{z}} \frac{\sqrt{\rho'} (y - y')}{\tilde{R}^{3/2}} \right) d\sigma \right|^2}{|Z_0 (\sin \theta \hat{\mathbf{y}} - \cos \theta \hat{\mathbf{z}})|^2}. \tag{193}$$

Recognizing that $\lim_{\rho' \rightarrow \infty} \sqrt{\rho'}/\sqrt{\tilde{R}} = 1$, and $\lim_{\rho' \rightarrow \infty} y/\tilde{R} = 0$, and again applying the geometry in Figure 4, this can be rewritten as

$$\sigma_{2\text{-D}} \approx 2\pi \frac{\left| \sqrt{\frac{1}{2j\pi k_0}} (-\sin(\theta) \hat{\mathbf{y}} + \cos(\theta) \hat{\mathbf{z}}) \int_{\sigma} \frac{\partial u}{\partial z} e^{jk_0 y \cos(\theta)} d\sigma \right|^2}{|(\sin \theta \hat{\mathbf{y}} - \cos \theta \hat{\mathbf{z}})|^2}. \tag{194}$$

Finally, converting the integral into a summation and simplifying the result reduces the RCS equation to

$$\sigma_{2-D} \approx \frac{1}{k_0} \left| \sum_{n=1}^{N_1} b_n \Delta_n e^{jk_0 y_{n+\frac{1}{2}} \cos(\theta)} \right|^2, \quad (195)$$

where the b_n are the approximations to $\frac{\partial u}{\partial z}$ on each segment, $\Delta_n = l_{n+1} - l_n$ is the length of each segment, $y_{n+\frac{1}{2}}$ is the matchpoint of each segment, and θ is the angle of incidence.

5.2 RCS Plots

The integral equation method is applied to several test cavities in this section, and the monostatic RCS signatures are computed for incident angles between 90° and 180° . The accuracy of the method is considered by comparing the plots with the RCS values calculated by RAM2D [7] as well as with the results from a hybrid finite element/Fourier transform code written by Van [25]. The RAM2D code is a commercial grade two-dimensional scattering problem solver, and Van's finite element code has been benchmarked against other existing known results.

5.2.1 Test Cavity 1. For the first test case, consider the cavity in Figure 5. It is a rectangular cavity with dimensions 1 meter wide by 0.25 meters deep. The interior of the cavity is unfilled, which is denoted by the free space parameters (ϵ_0, μ_0) . So in this case, $\epsilon_1 = \epsilon_0$ and $\mu_1 = \mu_0$. Let an incident plane wave under TE polarization and with frequency 300 MHz impinge on the cavity to produce the scattered fields. The incident wave will have a wavelength of $\lambda = 1$ meter, and its wave number or propagation constant will be $k = 2\pi$. Notice that since the cavity is unfilled, the incident field's propagation constant is the same in the upper half plane as it is within the interior of the cavity.

The MoM algorithm was employed using 10 pulse basis functions per wavelength. This results in having 10 segments on the aperture ($N_1 = 10$) and 16 segments on the surface of the cavity ($N_2 = 16$), making $Au = f$ a 36 by 36 linear system. The unknown expansion coefficients were approximated by the method to produce the total magnetic field on the perimeter of the cavity and the normal derivative of the total magnetic field on the aperture of the cavity. The magnitudes of these field quantities (in Amperes/meter)

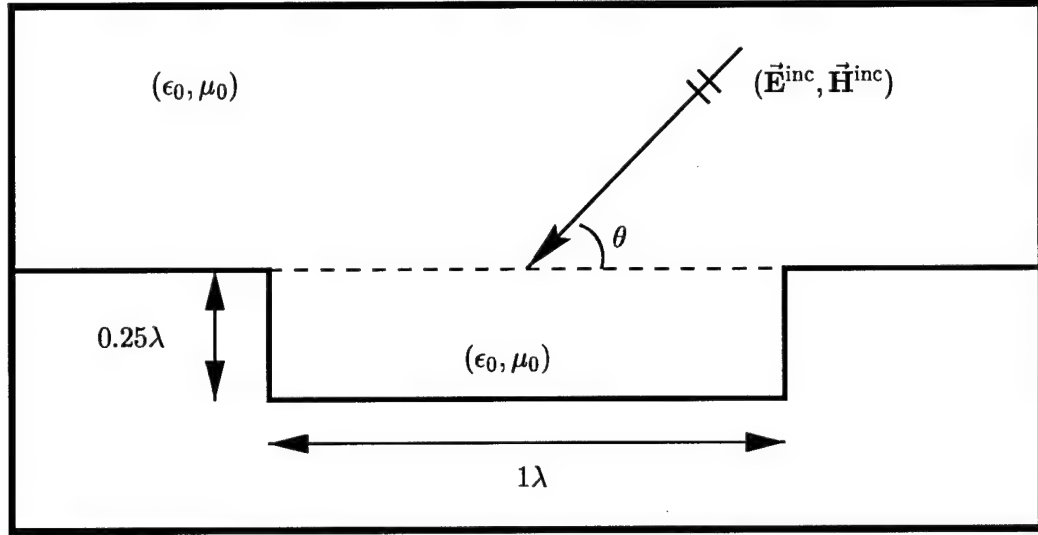


Figure 5 Geometry of unfilled rectangular cavity

are shown in Figures 6, 7, and 8 for an incident angle of $\theta = 90^\circ$. (It should be pointed out here that more than 10 pulse basis functions per wavelength were used to produce the plots of the fields in the following 3 figures. Actually, 25 pulses were used so that the graphs would be fairly smooth. However, only 10 pulses per wavelength were used to compute the RCS values.)

In Figures 6, 7, and 8 notice that the fields all have a symmetric shape with respect to the center of the cavity. This is to be expected when a symmetric cavity is illuminated by a plane wave at normal incidence. Finally, in Figure 9 the graph of the monostatic RCS values computed by the integral equation method is plotted for several angles between 90° and 180° . The integral equation method output is compared with the RCS values computed by RAM2D in the figure, and excellent agreement is observed. So the MoM algorithm was able to produce very accurate results while only having to solve a 36 by 36 linear system for each incident angle.

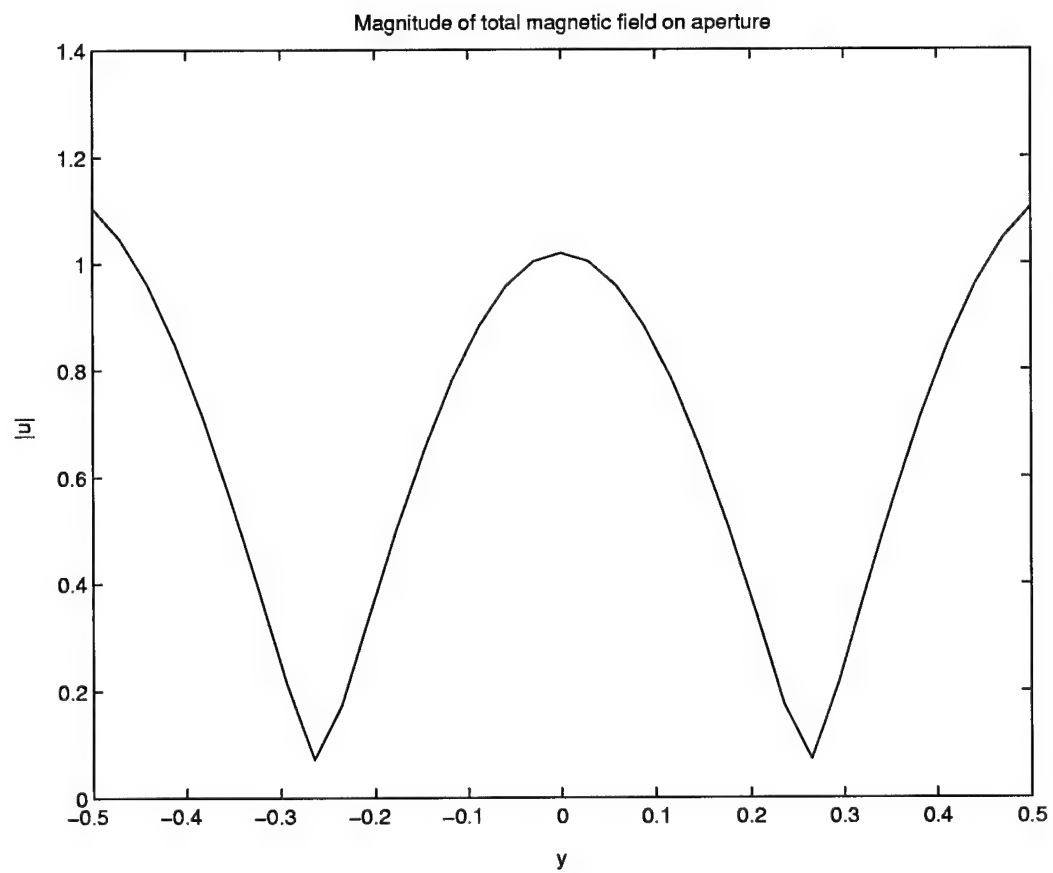


Figure 6 Magnitude of the total magnetic field on the aperture, normal incidence

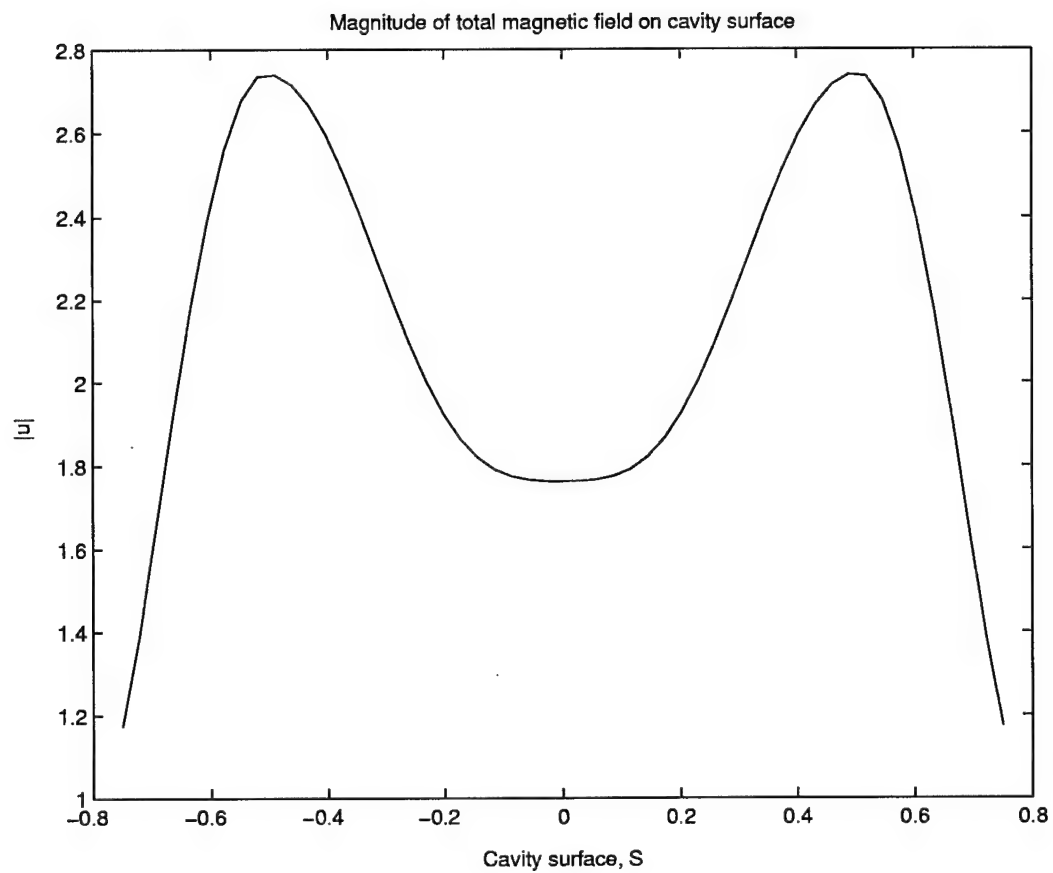


Figure 7 Magnitude of the total magnetic field on the cavity surface, normal incidence

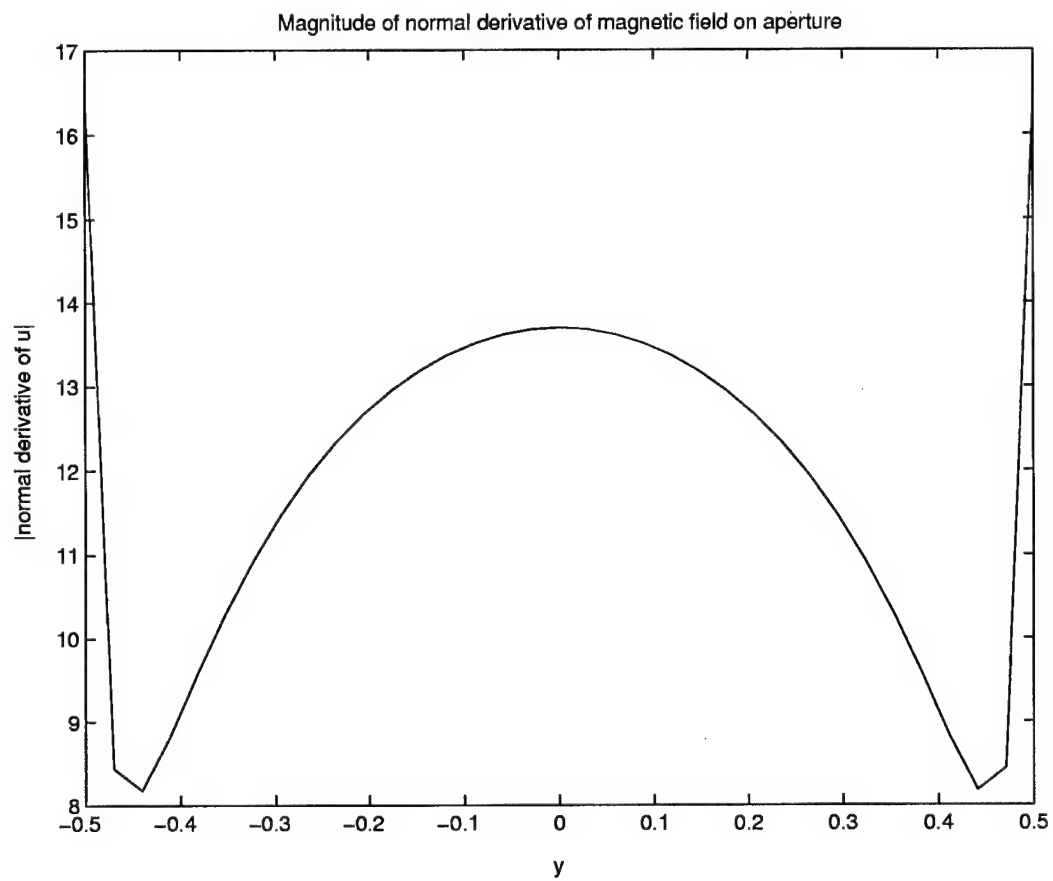


Figure 8 Magnitude of the normal derivative of the magnetic field on the aperture, normal incidence

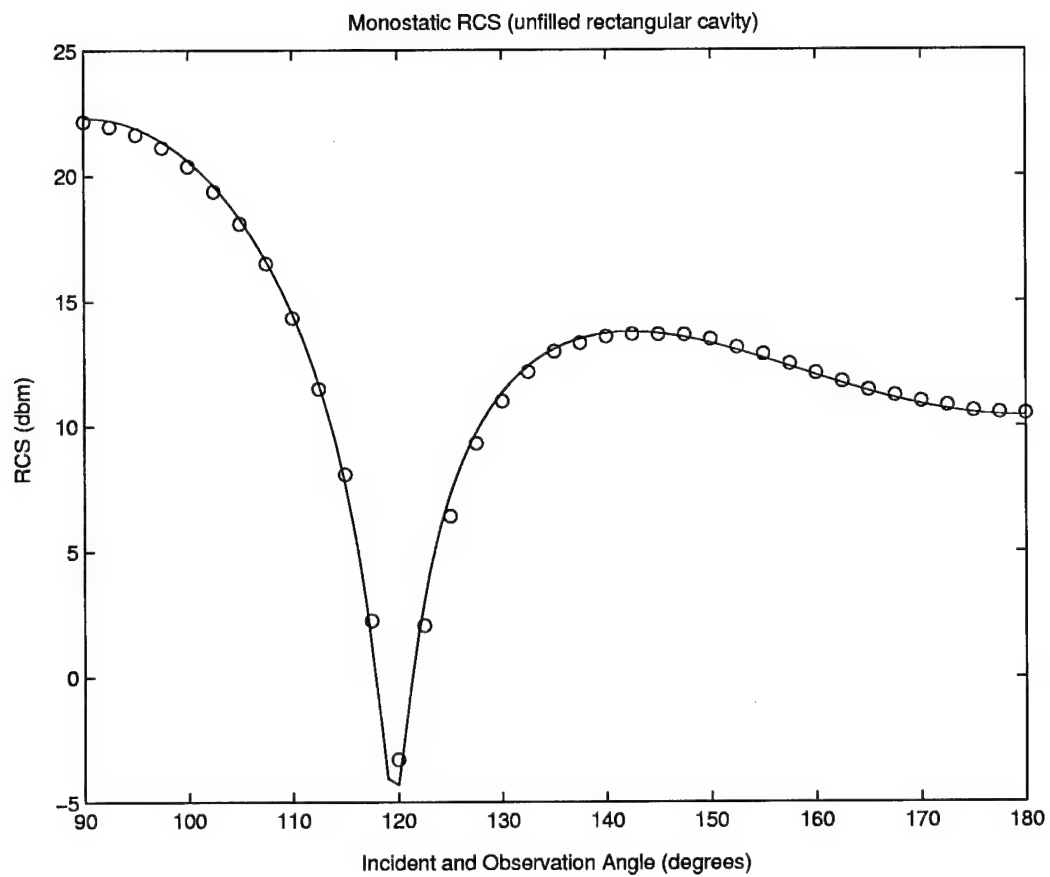


Figure 9 Monostatic RCS signature of an unfilled rectangular cavity. Integral equation method (o) and RAM2D (—)

5.2.2 Test Cavity 2. For the second test case, another unfilled rectangular cavity is illuminated by a 300 MHz plane wave under TE polarization. Consequently, the wavelength of the incident field is $\lambda = 1$ meter and the propagation constant is again $k = 2\pi$ both in the upper half plane and the interior of the cavity. However, this time the cavity is much deeper and a little bit wider. As shown in Figure 10, the cavity is 1.2 meters wide and 0.8 meters deep.

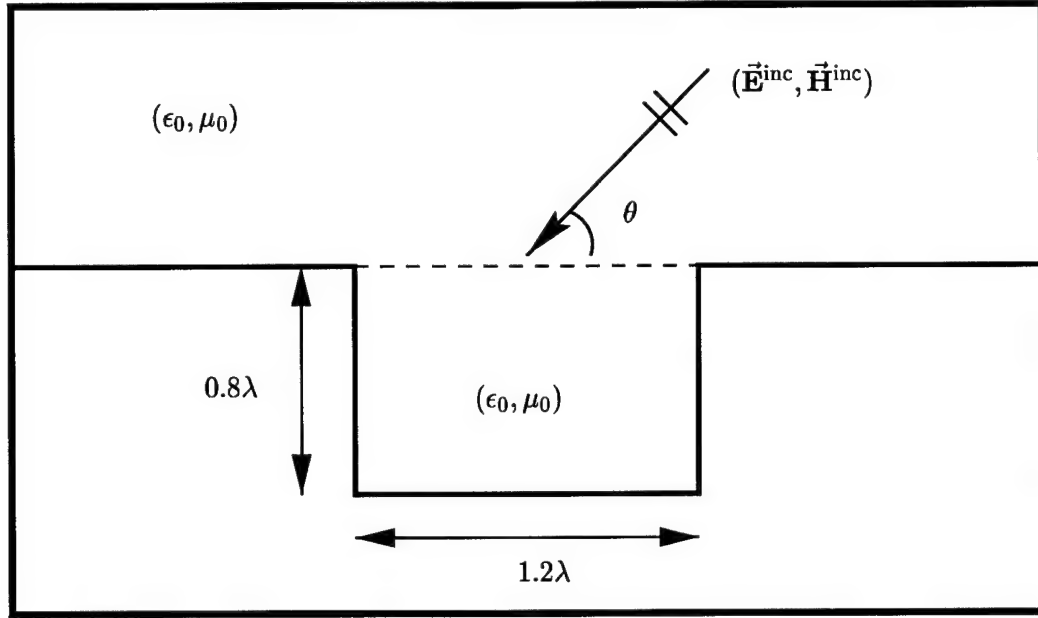


Figure 10 Geometry of a deep rectangular cavity

The MoM algorithm was again employed using 10 pulse basis functions per wavelength. Due to the geometry of the cavity, this resulted in a total of 12 segments on the cavity aperture ($N_1 = 12$) and 28 segments on the cavity surface ($N_2 = 28$). So the total number of unknown expansion coefficients is 52, making $Au = f$ a 52 by 52 linear system. Again, using equation (195) the monostatic RCS values were computed by the MoM algorithm for incident angles between 90° and 180° , and the results were compared to the RCS values computed by RAM2D. In Figure 11, the two sets of data are compared, and excellent agreement between the two methods is again observed.

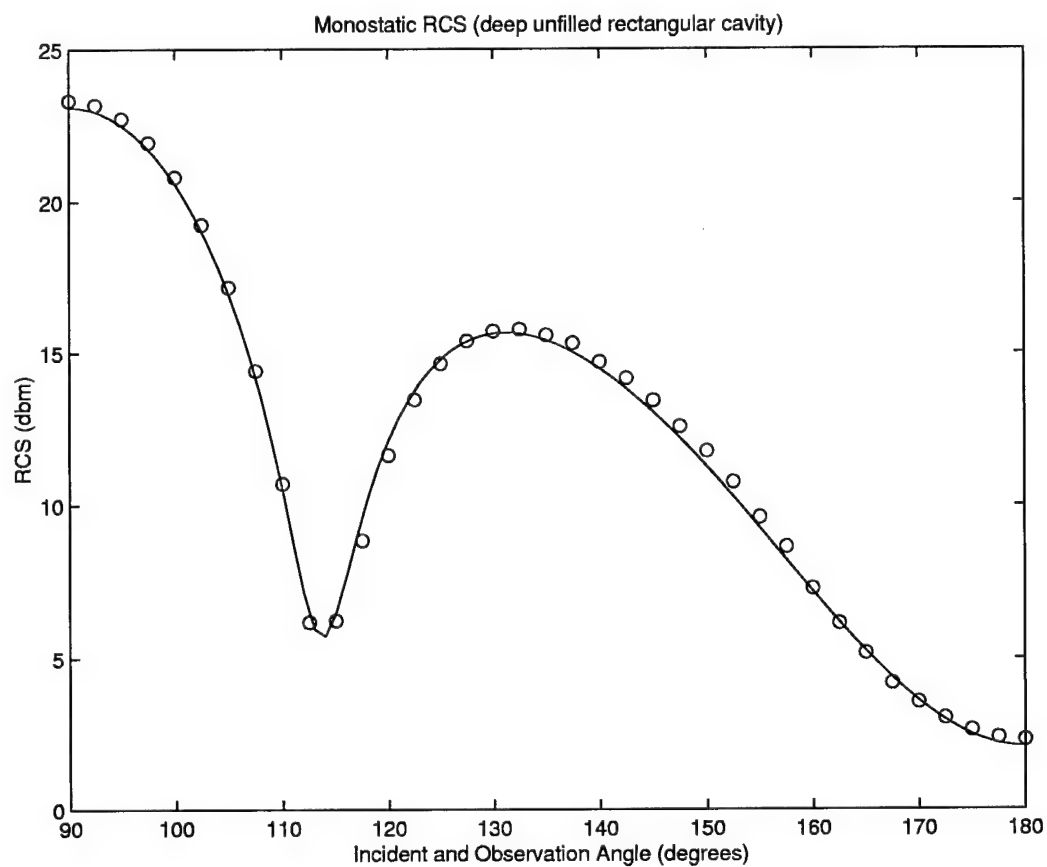


Figure 11 Monostatic RCS signature of a deep unfilled rectangular cavity. Integral equation method (o) and RAM2D (—)

5.2.3 Test Cavity 3. For the third test case, a rectangular cavity filled with a homogeneous, lossy material is considered. The incident field for the problem is still a TE polarized plane wave with frequency 300 MHz and wavelength $\lambda = 1$ meter. The propagation constant in the upper half plane is still $k_0 = 2\pi$, however the fields will have a different wave number within the cavity due to the presence of the lossy material. In this case, the cavity is filled with a lossy dielectric material characterized by $\epsilon_r = 4 - j$, so the propagation constant within the material filled cavity is $k_1 = 2\pi\sqrt{4 - j}$. The dimensions of the cavity are the same as the rectangular cavity from the first test case, 1 meter wide and 0.25 meters deep. The geometry of the problem is shown in Figure 12.

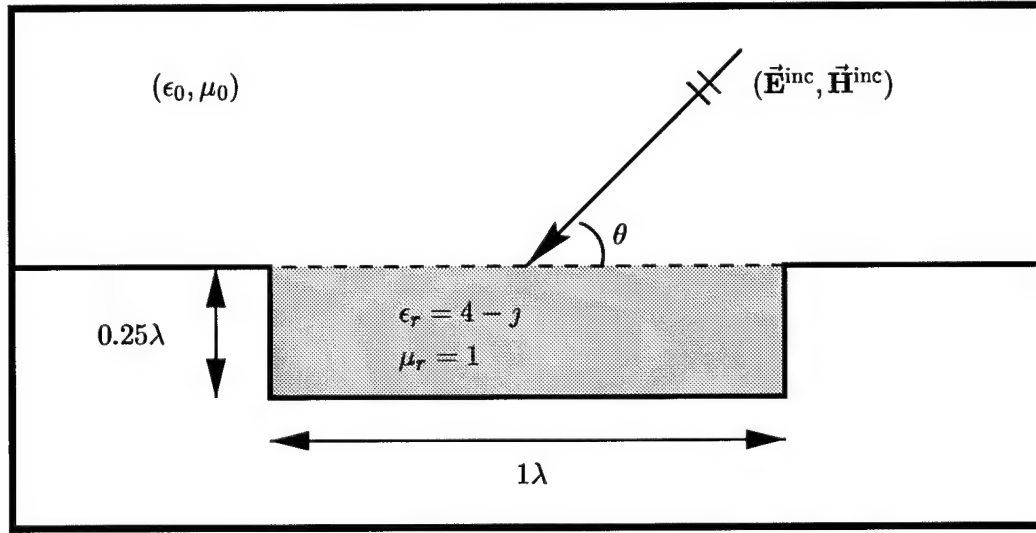


Figure 12 Geometry of a rectangular cavity filled with a lossy material

The monostatic RCS values were computed and compared with the results found by a hybrid finite element/Fourier transform code written by Van [25]. The plots appear in Figure 13 and indicate very good agreement between the two methods. In comparing the two RCS signatures in Figures 9 and 13, the effect of the lossy dielectric material appears to be fairly significant. Both graphs have a null appearing around $\theta = 120^\circ$ and have very similar overall shapes, but the RCS values for the filled case are much lower than for the unfilled case. This is because the dielectric material absorbs some of the energy of the incident field which results in a decreased scattered field.

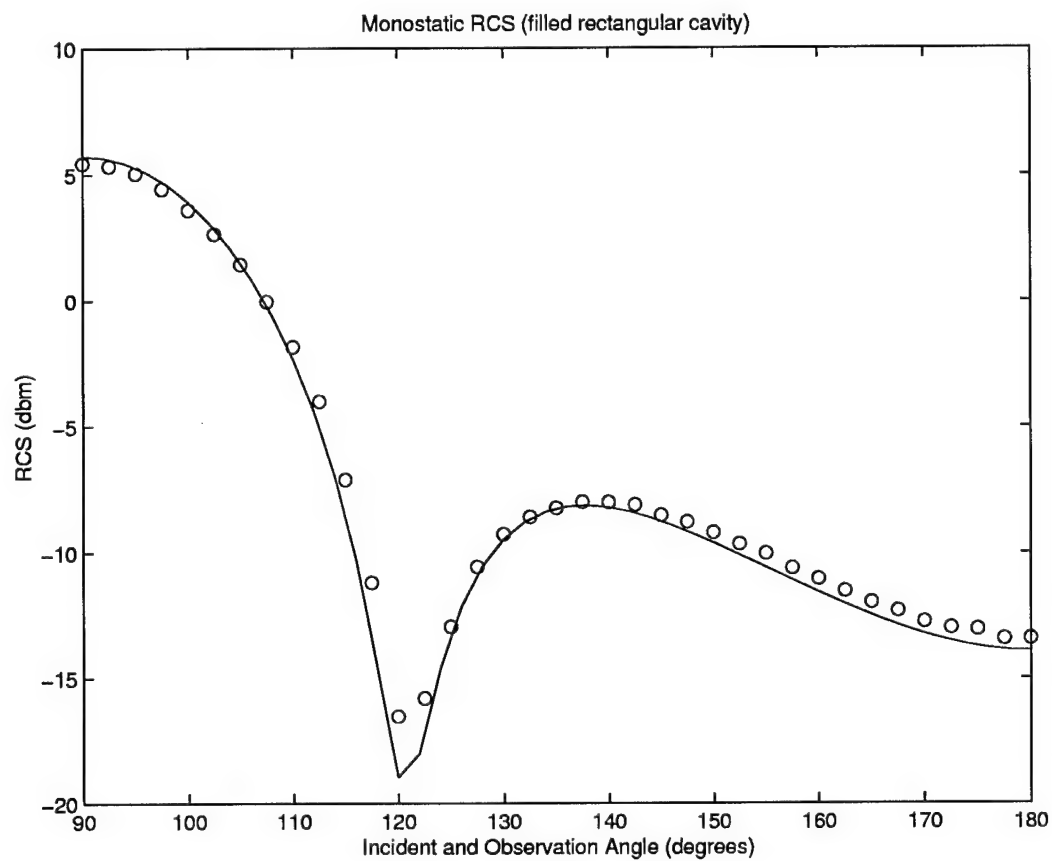


Figure 13 Monostatic RCS signature of a rectangular cavity filled with a lossy dielectric material. Integral equation method (o) and finite element method (—)

5.2.4 Test Cavity 4. The fourth test cavity is a deep rectangular cavity filled with a homogeneous, lossy dielectric material. Again, the incident field is a TE polarized plane wave with frequency 300 MHz. The relative electric permittivity of the medium is $\epsilon_r = 2 - j$ which makes the wave number $k_1 = 2\pi\sqrt{2 - j}$ inside the cavity interior. In the upper half plane, the propagation constant is still $k_0 = 2\pi$, and the incident field has a wavelength of $\lambda = 1$ meter. The geometry of the fourth test case is shown in Figure 14. The cavity is 1.2 meters wide and 0.8 meters deep.

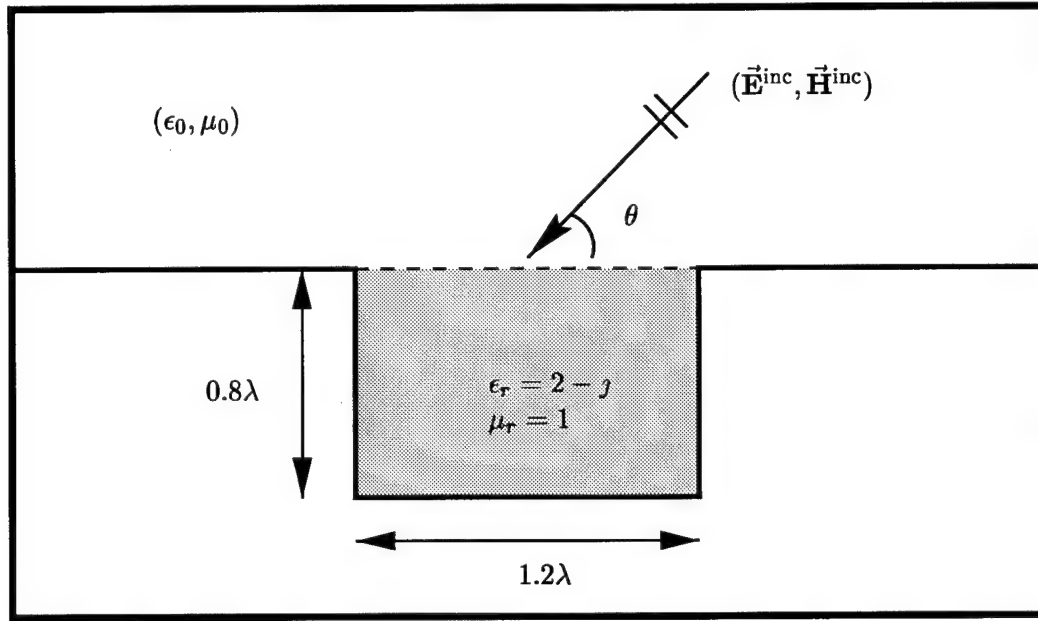


Figure 14 Geometry of a deep rectangular cavity filled with a lossy material

The MoM algorithm was employed using 10 pulse basis functions per wavelength. This resulted in solving a 52 by 52 linear system for each incident angle. The RCS values given by the integral equation method as well as a comparison with Van's finite element/Fourier transform method are shown in Figure 15. Again, for a very small computational effort, strong agreement is observed between the two methods.

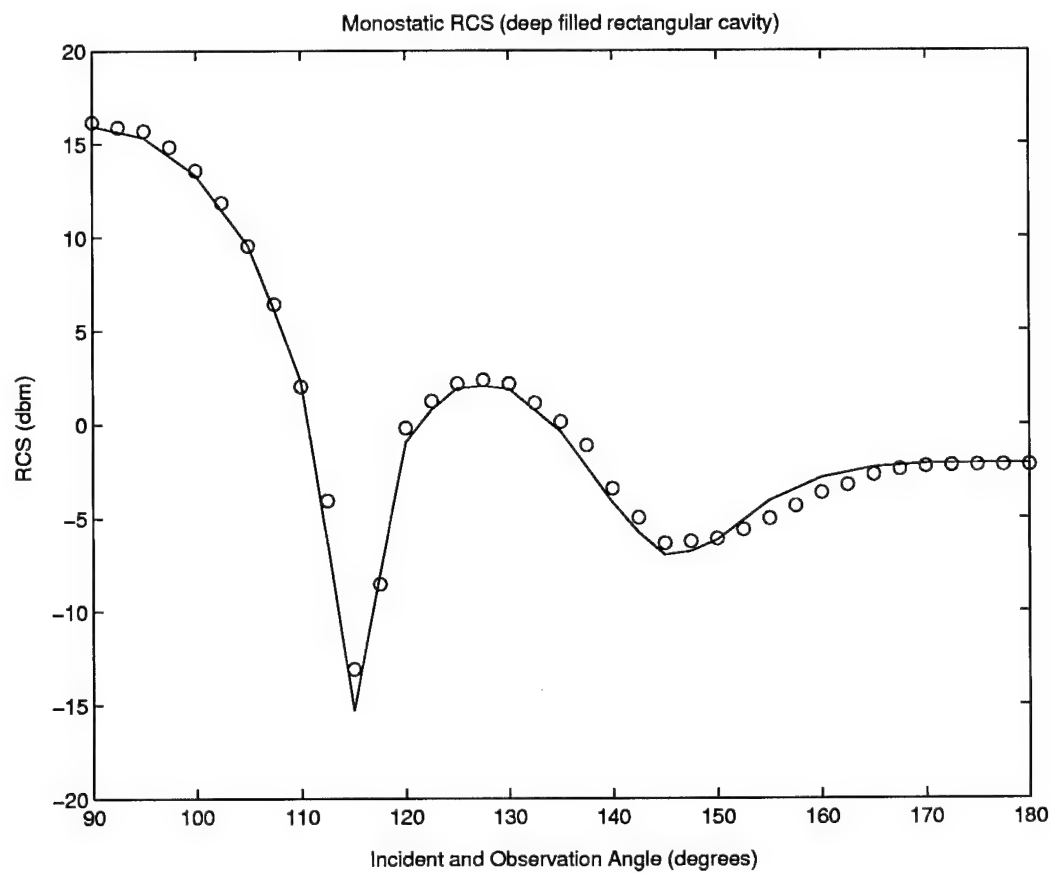


Figure 15 Monostatic RCS signature of a deep rectangular cavity filled with a dielectric material. Integral equation method (o) and finite element method (—)

5.2.5 Test Cavity 5. The final test cavity is a triangular shaped cavity filled with a homogeneous, lossy dielectric material. The dimensions of the triangular cavity are 1 meter wide across the aperture and 0.5 meters deep. The interior of the cavity is filled with a dielectric material having relative electric permittivity $\epsilon_r = 4 - j$. This makes the wave number in the interior of the cavity $k_1 = 2\pi\sqrt{4 - j}$. The incident field is a 300 MHz plane wave under TE polarization. Again, the wavelength of the incident field is $\lambda = 1$ meter, and its free space propagation constant is $k_0 = 2\pi$. The geometry of the fifth test case appears in Figure 16.

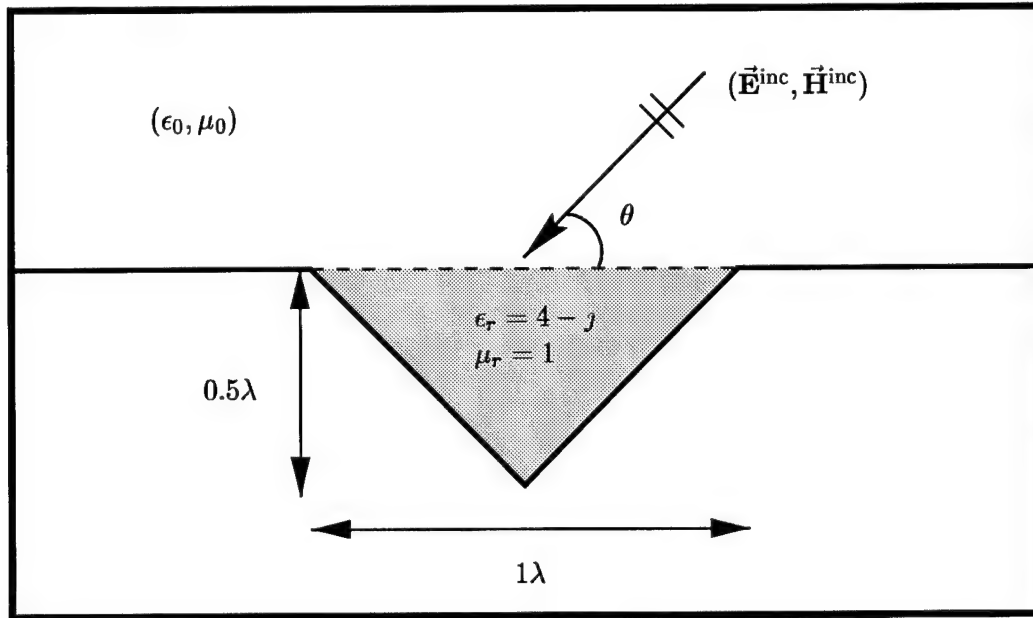


Figure 16 Geometry of a triangular cavity filled with a lossy material

Using 10 pulse basis functions per wavelength, the perimeter of the cavity is discretized into 10 segments along the aperture and 16 segments along the surface. This results in the MoM algorithm solving a 36 by 36 linear system for each incident angle. Comparing the RCS values of the integral equation method with those found by the finite element/Fourier transform method in Figure 17 again shows very good agreement.

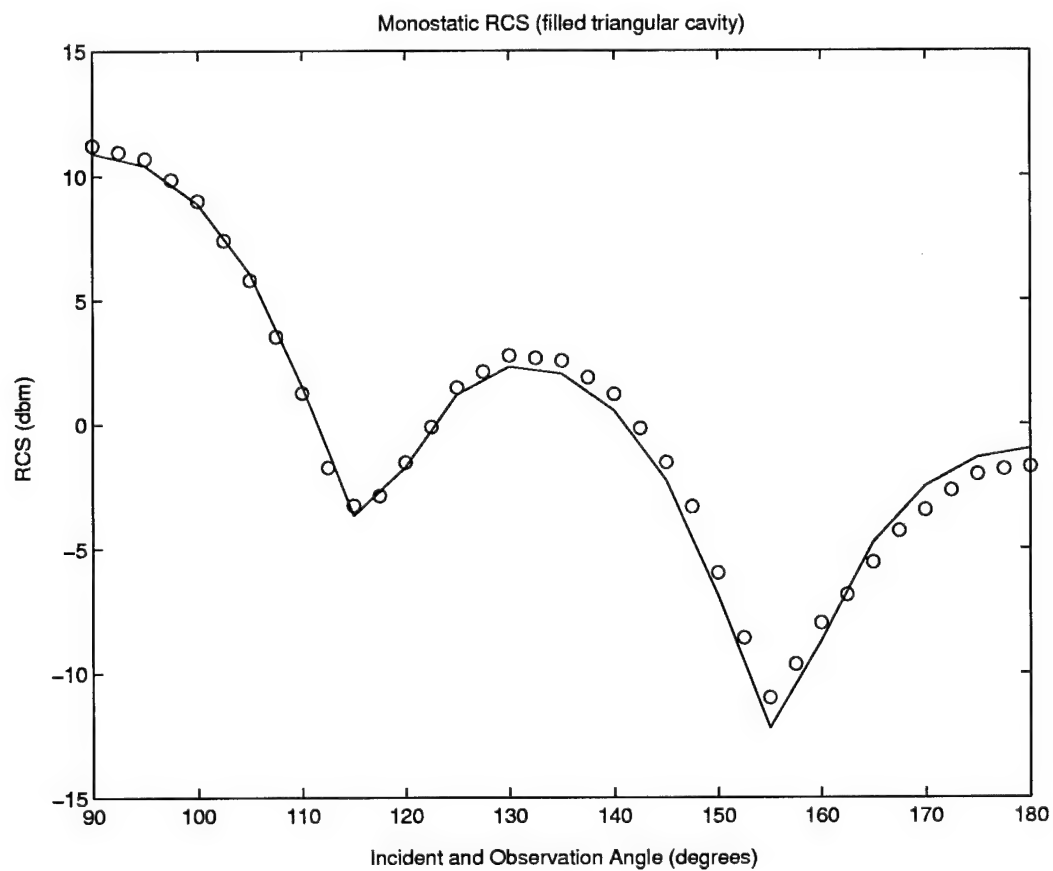


Figure 17 Monostatic RCS signature of a triangular cavity filled with a dielectric material. Integral equation method (o) and finite element method (—)

5.3 Error History Plots

In this section, the rate of convergence of the integral equation method is examined. In the following experiments, each cavity is initially meshed with N equally sized segments of length h , and the MoM algorithm is used to compute the total magnetic field along the cavity boundary ∂D . Then, the mesh is refined by chopping each segment in half so that there are a total of $2N$ segments along ∂D , and the total magnetic field is recomputed. At each step the relative error in the L^2 -norm is computed using the formula

$$\text{error}_n = \frac{\|u_{h_n} - u_{h_{n-1}}\|_{L^2}}{\|u_{h_n}\|_{L^2}} \quad (196)$$

where $h_n = h_{n-1}/2$ indicating that the mesh is chopped in half at each step, u_{h_n} is the approximate solution at the current size step, and $u_{h_{n-1}}$ is the approximate solution at the previous size step.

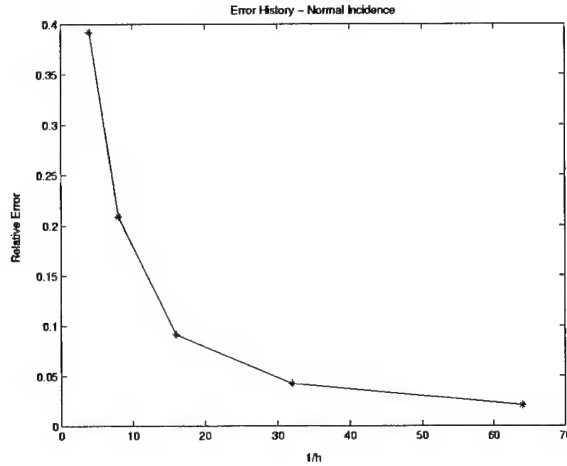


Figure 18 Relative error history of an empty rectangular cavity for normal incidence

Test Case 1. For the first experiment, consider the scattering from an unfilled cavity 1 meter wide by 0.25 meters deep of a 300 MHz plane wave under TE polarization. Let the plane wave impinge on the cavity under normal incidence ($\theta = 90^\circ$). Using equation (196), the relative error history versus $1/h$ is plotted in Figure 18, and a \log_2 - \log_2 plot of the relative error versus $1/h$ is given in Figure 19.

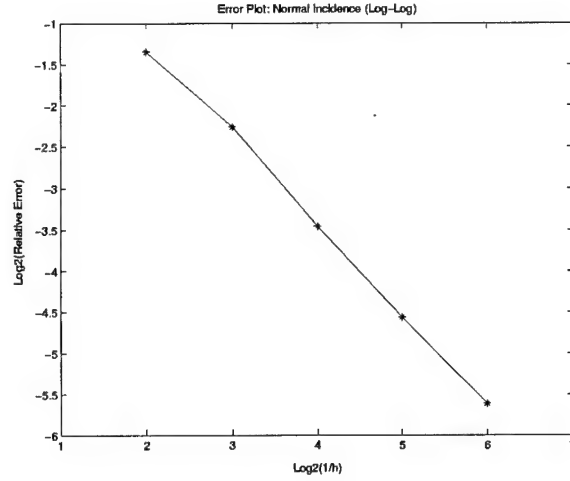


Figure 19 Log-Log plot of relative error history for normal incidence

Notice in Figure 18 that at each size step where h is halved, the relative error seems to be cut approximately in half. So for h sufficiently small the L^2 error rate is approaching 1 for the solution of an unfilled rectangular cavity under normal incidence. Furthermore, the slope of the line in Figure 19 is approximately -1.07 which is indicative of an $\mathcal{O}(h)$ method. This agrees with the estimate given in the previous chapter.

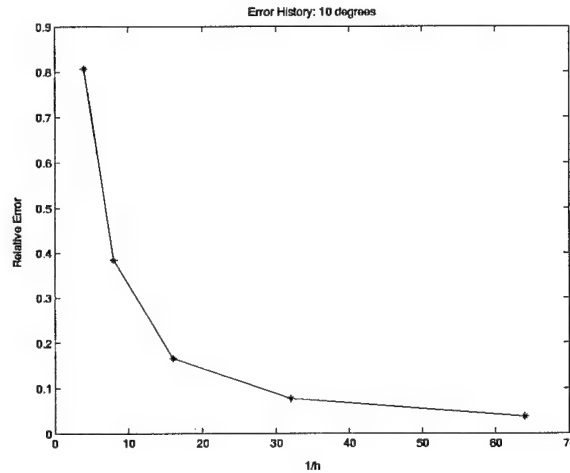


Figure 20 Relative error history of an empty rectangular cavity, $\theta = 10^\circ$

Test Case 2. In this experiment, consider the same cavity as in Test Case 1 with a 300 MHz plane wave under TE polarization impinging on the cavity at an incident angle of $\theta = 10^\circ$. According to Figure 20, the L^2 error rate also appears to be approaching 1 for

this case as the mesh is refined at each size step. And the slope of the line in Figure 21 is approximately -1.1 which again agrees with the rate of convergence estimate.

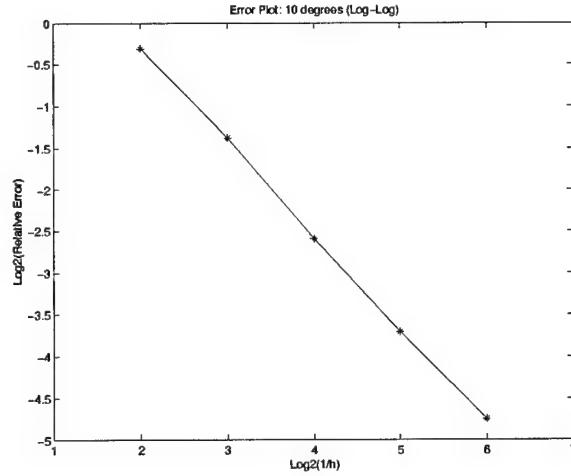


Figure 21 Log-Log plot of relative error history, $\theta = 10^\circ$

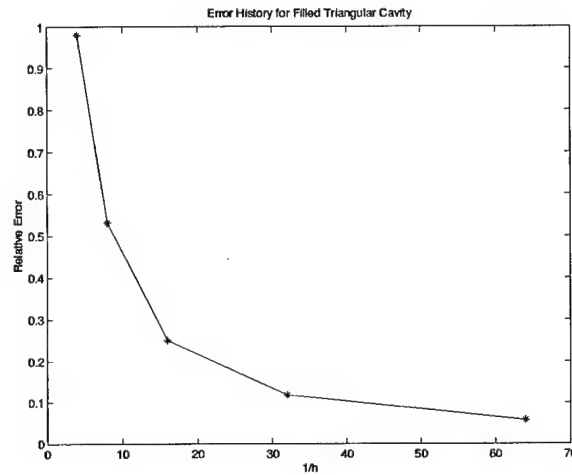


Figure 22 Relative error history of a filled triangular cavity, $\theta = 35^\circ$

Test Case 3. In this experiment, a filled triangular cavity is considered. The cavity is in the shape of an isosceles triangle 1.2 meters by 0.8 meters deep. It is filled with a dielectric material having relative electric permittivity $\epsilon_r = 2.26$. Again the incident wave is a TE polarized plane wave with frequency 300 MHz, and it is propagating at an incident angle of $\theta = 35^\circ$. The relative error plot in Figure 22 again indicates that for h sufficiently small, the rate of convergence is approaching 1 since the relative error is cut approximately in

half at each step. Also, the $\log_2\text{-}\log_2$ plot of the relative error versus $1/h$ in Figure 23 shows a slope of about -1.02 which is consistent with an $\mathcal{O}(h)$ rate of convergence.

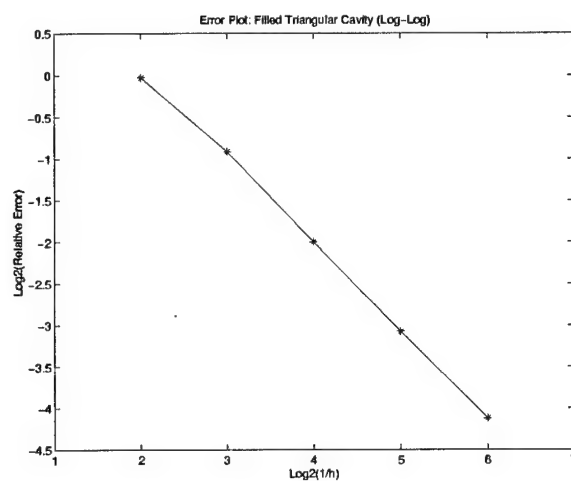


Figure 23 Log-Log plot of relative error for a filled triangular cavity, $\theta = 35^\circ$

VI. Conclusions

This research has investigated the application of a moment method based integral equation scheme to compute the scattering of a TE polarized plane wave from a cavity embedded in a PEC ground plane. This is motivated primarily by the need of the United States military to accurately model and predict the RCS signatures of targets. The reduction and/or enhancement of a friendly air vehicle's RCS signature as well as the detection and identification of an enemy air vehicle are crucial to the success of an air campaign. Cavities on an aircraft, such as the jet engine inlet ducts and exhaust nozzles, can dominate its RCS signature. This coupled with the challenging computational nature of cavities make the study of the scattering from cavities vitally important.

There is a large body of research regarding the cavity scattering problem, and there are many good methods for computing the RCS of cavities. Among these are the generalized network formulation (GNF), integral equation methods such as the electric field integral equation (EFIE) method and the magnetic field integral equation (MFIE) method, and the hybrid finite element methods. One of the primary advantages of the method presented here is that it does not suffer from the problem of spurious resonances at certain frequencies like some of the other methods. Also, it is very computationally efficient since only the boundary of the cavity must be meshed to solve the problem. Once the fields along the boundary of the cavity are found, the fields everywhere above the cavity can be computed for applications such as capturing the RCS signature of the cavity. So very accurate results can be produced with a minimal amount of computations required.

In the previous chapters, the fundamental theorems developed in [4] and [26] were converted to vector integral equations that govern the electromagnetic scattering from a cavity embedded in a PEC ground plane. A coupled set of scalar integral equations were then derived for the problem of a TE polarized plane wave impinging on a two-dimensional cavity, where the cavity could either be empty or filled with a homogeneous material. These scalar integral equations were then solved via a Method of Moments algorithm, and the RCS signatures of several test cavities were computed. The results produced compared very well with the results of other methods including RAM2D and a finite element method code, and in doing so, the method was very computationally efficient. An estimate of the

order of convergence of the method was also developed, and the numerical results indicated that it was an accurate estimate.

This research represents a follow-on effort to work previously accomplished by Asvestas, Kleinman, Wood, and Wood [4], [26], [27], but the problem certainly has not been exhausted. There are several areas where future research could be accomplished. First, instead of simply having an empty or filled cavity, a thin dielectric coating on the surface of the cavity could be modeled or a cavity filled with layers of different materials. Also, another area of research would be in comparing the rate of convergence of the method with the rates of other methods. Furthermore, while the method has been shown to produce accurate results, it would be useful to prove that the method always obtains the unique solution to the scattering problem. Finally, the problem considered in this research could be extended to the three-dimensional case, since the integral equations are valid in both two and three dimensions.

Bibliography

1. Ammari, Habib, Gang Bao, and Aihua W. Wood. "A cavity problem for Maxwell's equations," preprint.
2. Ammari, Habib, Gang Bao, and Aihua W. Wood. "An integral equation method for the electromagnetic scattering from cavities," *Mathematical Methods in the Applied Sciences*, vol. 23, pp. 1057-1072, 2000.
3. Ammari, Habib, Gang Bao, and Aihua W. Wood. "Analysis of the electromagnetic scattering from a cavity," preprint.
4. Asvestas, J. S. and R. E. Kleinman. "Electromagnetic scattering by indented screens," *IEEE Transactions on Antennas and Propagation*, vol. 42, pp. 22-30, 1994.
5. Atkinson, Kendall E. *An Introduction to Numerical Analysis*. New York: John Wiley and Sons, 1989.
6. Balanis, Constantine A. *Advanced Engineering Electromagnetics*. New York: John Wiley and Sons, 1989.
7. Clary, R. L. "RAM2D: Two-dimensional integral equation computer code, version 3.0," *Northrop Grumman Corporation*, 1995.
8. Collins, Peter. Class notes distributed in EENG 630: Applications of Electromagnetic Theory, Graduate School of Engineering, Air Force Institute of Technology (AETC), Wright-Patterson AFB OH, Spring 2001.
9. Davis, Harry F. and Arthur David Snider. *Introduction to Vector Analysis*. Dubuque, IA: Wm. C. Brown Publishers, 1991.
10. Ford, Arthur Peyton, IV. *Computation of Scattering From Bodies of Revolution Using an Entire-Domain Basis Implementation of the Moment Method*. Thesis, Graduate School of Engineering, Air Force Institute of Technology (AETC), Wright-Patterson AFB OH, March 1999.
11. Goggans, Paul M. and Thomas H. Shumpert. "Backscatter RCS for TE and TM excitations of dielectric-filled cavity-backed apertures in two-dimensional bodies," *IEEE Transactions on Antennas and Propagation*, vol. 39, pp. 1224-1227, 1991.
12. Harrington, Roger F. *Field Computation by Moment Methods*. New York: The Macmillan Company, 1968.
13. Harrington, Roger F. *Time-Harmonic Electromagnetic Fields*. New York: McGraw-Hill Publishing, 1961.
14. Harrington, R. F. and J. R. Mautz. "A generalized network formulation for aperture problems," *IEEE Transactions on Antennas and Propagation*, pp. 870-873, 1976.
15. Jackson, John D. *Classical Electrodynamics*. New York: John Wiley and Sons, 1999.
16. Jeng, S.K. "Scattering from a cavity-backed slit in a ground plane - TE case," *IEEE Transactions on Antennas and Propagation*, vol 38, pp. 1523-1529, 1990.

17. Jin, Jian-Ming. *The Finite Element Method in Electromagnetics*. New York: John Wiley and Sons, 1993.
18. Jin, Jian-Ming and John L. Volakis. "A finite element-boundary integral formulation for scattering by three-dimensional cavity-backed apertures," *IEEE Transactions on Antennas and Propagation*, vol. 39, pp. 97-104, 1991.
19. Kempel, Leo C. and Thomas B. A. Senior. "Scattering by a small cavity backed hole," *IEEE Transactions on Antennas and Propagation*, vol. 41, pp. 1115-1121, 1993.
20. Kreyszig, Erwin. *Advanced Engineering Mathematics*. New York: John Wiley and Sons, 1993.
21. Liang, C. H. and D. Cheng. "Electromagnetic fields coupled into a cavity with a slot-aperture under resonant conditions," *IEEE Transactions on Antennas and Propagation*, vol. 30, pp. 664-672, 1982.
22. Rahman, B. M. A. "Penalty function improvement of waveguide solution by finite elements," *IEEE Transactions of Microwave Theory and Techniques*, vol. 32, pp. 922-928, 1984.
23. Rao, Sadasiva M., Griffin K. Gothard, and Donald R. Wilton. "Application of finite-integral technique to electromagnetic scattering by two-dimensional cavity-backed aperture in a ground plane," *IEEE Transactions on Antennas and Propagation*, vol. 46, pp. 679-685, 1998.
24. Reuster, D.H. and G.A. Thiele. "A field iterative method for computing the scattered electric fields at the apertures of large perfectly conducting cavities," *IEEE Transactions on Antennas and Propagation*, vol. 43, pp. 286-290, 1995.
25. Van, Tri and Aihua W. Wood. "Finite Element Analysis of Electromagnetic Scattering From a Cavity," preprint.
26. Wood, William D. *Electromagnetic Scattering from a Cavity in a Ground Plane: Theory and Experiment*. PhD dissertation, Graduate School of Engineering, Air Force Institute of Technology (AETC), Wright-Patterson AFB OH, March 1997.
27. Wood, William D. and Aihua W. Wood. "Development and Numerical Solution of Integral Equations for Electromagnetic Scattering from a Trough in a Ground Plane," *IEEE Transactions on Antennas and Propagation*, vol. 47, pp. 1318-1322, 1999.